

Contents lists available at ScienceDirect

Journal of Computational Physics

www.elsevier.com/locate/jcp



A spectral boundary integral method for the elastic obstacle scattering problem in three dimensions *



Heping Dong^a, Jun Lai^{b,*}, Peijun Li^c

- ^a School of Mathematics, Jilin University, Changchun, Jilin 130012, China
- ^b School of Mathematical Sciences, Zhejiang University Hangzhou, Zhejiang 310027, China
- ^c Department of Mathematics, Purdue University, West Lafayette, IN 47907, USA

ARTICLE INFO

Article history: Received 26 March 2022 Accepted 13 August 2022 Available online 22 August 2022

Keywords: Navier equation Elastic scattering problem Boundary integral equation Spherical harmonics

ABSTRACT

In this paper, we consider the scattering of a plane wave by a rigid obstacle embedded in a homogeneous and isotropic elastic medium in three dimensions. Based on the Helmholtz decomposition, the elastic scattering problem is reduced to a coupled boundary value problem for the Helmholtz and Maxwell equations. A novel system of boundary integral equations is formulated and a spectral boundary integral method is developed for the coupled boundary value problem. Numerical experiments are presented to demonstrate the superior performance of the proposed method.

© 2022 Elsevier Inc. All rights reserved.

1. Introduction

The scattering problems for elastic waves have attracted considerable attention due to the significant applications in diverse scientific areas such as nondestructive testing, medical imaging, and seismic exploration [1,16]. Although many mathematical and computational results are available, it still presents a challenging question on accurate computing of the scattering problems for elastic waves, especially in three dimensions, due to the complexity of the underlying equation. This paper is concerned with a numerical solution for the time-harmonic elastic scattering problem of a rigid obstacle embedded in a homogeneous and isotropic elastic medium in three dimensions. The goal is to develop a spectral boundary integral method for the elastic obstacle scattering problem.

Compared with the finite element or finite difference methods, the method of boundary integral equations has two intrinsic advantages: it is only required to discretize the boundary of the domain and the radiation condition at infinity is satisfied automatically [21,23]. However, it also brings an extra difficulty that boundary integrals are usually singular and their accurate numerical approximation is highly involved, especially for three dimensional geometries. Over the years, various methods of boundary integral equations have been proposed to solve the three-dimensional elastic scattering problems. A high order singular integral quadrature method with GMRES was developed in [3] for the elastic scattering problems with the Dirichlet and Neumann boundary conditions on closed and open surfaces. In [4], the elastic wave scattering of a time-harmonic incident wave that impinges on a penetrable obstacle was considered, and the singular integral was discretized

E-mail addresses: dhp@jlu.edu.cn (H. Dong), laijun6@zju.edu.cn (J. Lai), lipeijun@math.purdue.edu (P. Li).

^{*} The first author is supported by the NSFC grant 12171201 and the National Key Research and Development Program of China (grant No.2020YFA0713602). The second author JL was partially supported by the Funds for Creative Research Groups of NSFC (No. 11621101), NSFC grant U21A20425 and NSFC grant 11871427. JL was also supported by the "Xiaomi Young Scholars" program from Xiaomi Foundation. The third author was supported in part by the NSF grant DMS-1912704 and NSF grant DMS-2208256.

^{*} Corresponding author.

by the use of partition of unity. Based on the fact that for analytic functions on a smooth closed surface that is isomorphic to a sphere and the interpolation based on spherical harmonics gives spectral accuracy, a high order method for singular integrals in the boundary integral equation was developed in [10] and [12] for the acoustic wave equation and Maxwell's equations, respectively. In [19], a high order spectral method was proposed for solving elastic obstacle scattering problem with the Dirichlet or Neumann boundary condition by directly utilizing the Green function of the three-dimensional elastic wave equation.

It is worth mentioning that the Green function of the elastic wave equation is a second order tensor and the singularity is tedious to be separated in the computation of boundary integral equations, especially for the Neumann boundary condition and the three-dimensional problem [2–4,18,19,24]. To bypass this complexity, we employ the Helmholtz decomposition by introducing one scalar potential function and one vector potential function to split the displacement of the elastic wave field into the compressional and shear wave components. The two wave components, one of which satisfies the three-dimensional Helmholtz equation and the other one satisfies the Maxwell equation, are coupled at the boundary of the obstacle. Therefore, the boundary value problem of the elastic wave equation is converted equivalently into a coupled boundary value problem of the Helmholtz and Maxwell equations for the potentials. Such a decomposition greatly reduces the complexity for the computation of the elastic scattering problem. Similar techniques have also been successfully applied to many other problems such as the unsteady and incompressible flow, the two-dimensional elastic scattering, and inverse scattering problems [7–9,14,17,25].

In this work, by making use of the Helmholtz decomposition, the elastic obstacle scattering problem is reduced to a coupled boundary value problem, which is shown to have a unique solution. Based on the potential theory for the Helmholtz and Maxwell equations, a system of boundary integral equations is formulated for the coupled boundary value problem, and the uniqueness of the solution is discussed for the boundary integral formulation. For the numerical discretization, we adopt the Galerkin method and use the surface differential operators and Stokes' formula to reduce the strong singular operators to weakly singular ones. The approach leads to a high order full-discrete scheme which is similar to the one developed for the acoustic obstacle scattering problem in three dimensions [10]. It should be emphasized that all operations in the full discretization scheme are scalar, which greatly simplify the numerical implementation. Numerical experiments are provided for various geometries and different wavenumbers to demonstrate the superior performance of the proposed method.

To summarize, the paper contains three contributions:

- (1) propose a novel boundary integral formulation for the elastic boundary value problem via the Helmholtz decomposition;
- (2) regularize the singularity of the boundary integral by making use of the Stokes' formula and surface differential operators:
- (3) develop a spectral method for the approximation of the coupled boundary integral equations by using spherical harmonics.

The paper is organized as follows. In Section 2, we introduce the elastic scattering problem and reduce it to a coupled boundary value problem by using the Helmholtz decomposition. In Section 3, the system of coupled boundary integral equations is presented and the uniqueness is examined for the solution. Section 4 gives the spherical parameterization of the surface integral and discusses the regularization of the strong singular operators. The full-discrete spectral scheme is proposed in Section 5 for the system of the coupled boundary integral equations. Numerical experiments are shown in Section 6 to demonstrate the effectiveness of the proposed method. The paper concludes with some general remarks in Section 7.

2. Problem formulation

Consider a three-dimensional elastically rigid obstacle, which is given as a bounded domain $D \subset \mathbb{R}^3$ with analytic boundary Γ_D . Denote by ν the unit normal vector and τ_1, τ_2 the orthonormal tangential vectors on Γ_D , respectively. The exterior domain $\mathbb{R}^3 \setminus \overline{D}$ is assumed to be filled with a homogeneous and isotropic elastic medium with a unit mass density.

Let the obstacle be illuminated by a time-harmonic wave given explicitly by either the compressional plane wave $\boldsymbol{u}^i(x) = \boldsymbol{d}e^{\mathrm{i}\kappa_{\mathfrak{p}}\boldsymbol{d}\cdot x}$ or the shear plane wave $\boldsymbol{u}^i(x) = \boldsymbol{d} \times \boldsymbol{p}e^{\mathrm{i}\kappa_{\mathfrak{p}}\boldsymbol{d}\cdot x}$, where $\boldsymbol{d} = (\sin\theta\cos\varphi,\sin\theta\sin\varphi,\cos\theta)^{\top}$ is the unit propagation direction vector with $\theta \in [0,\pi], \varphi \in [0,2\pi)$ being the incident angles, \boldsymbol{p} is the unit polarization vector satisfying $\boldsymbol{p} \cdot \boldsymbol{d} = 0$, and

$$\kappa_{\mathfrak{p}} = \frac{\omega}{\sqrt{\lambda + 2\mu}}, \quad \kappa_{\mathfrak{s}} = \frac{\omega}{\sqrt{\mu}}$$

are the compressional and shear wavenumbers, respectively. Here $\omega > 0$ is the angular frequency and λ, μ are the Lamé constants satisfying $\mu > 0, \lambda + \mu > 0$. It can be verified that the incident wave \mathbf{u}^i satisfies the Navier equation

$$\mu \Delta \mathbf{u}^i + (\lambda + \mu) \nabla \nabla \cdot \mathbf{u}^i + \omega^2 \mathbf{u}^i = 0$$
 in \mathbb{R}^3 .

The displacement of the total field \boldsymbol{u} satisfies the Navier equation

$$\mu \Delta \mathbf{u} + (\lambda + \mu) \nabla \nabla \cdot \mathbf{u} + \omega^2 \mathbf{u} = 0 \text{ in } \mathbb{R}^3 \setminus \overline{D}.$$

The total field \boldsymbol{u} consists of the incident field \boldsymbol{u}^i and the scattered field \boldsymbol{v} , i.e.,

$$u=u^i+v$$
.

Since the obstacle is assumed to be rigid, we have

$$\mathbf{u} = 0$$
 on Γ_D .

Hence the scattered field \boldsymbol{v} satisfies the boundary value problem

$$\begin{cases} \mu \Delta \mathbf{v} + (\lambda + \mu) \nabla \nabla \cdot \mathbf{v} + \omega^2 \mathbf{v} = 0 & \text{in } \mathbb{R}^3 \setminus \overline{D}, \\ \mathbf{v} = -\mathbf{u}^i & \text{on } \Gamma_D. \end{cases}$$
(2.1)

For any solution \mathbf{v} of the Navier equation in (2.1), it has the Helmholtz decomposition

$$\mathbf{v} = \mathbf{v}_{\mathrm{p}} + \mathbf{v}_{\mathrm{s}},\tag{2.2}$$

where

$$\mathbf{v}_{\mathfrak{p}} = \nabla \phi, \quad \mathbf{v}_{\mathfrak{s}} = \mathbf{curl} \boldsymbol{\psi}, \quad \nabla \cdot \boldsymbol{\psi} = 0.$$

Here v_p and v_s are known as the compressional and shear wave components of v, respectively. Combining (2.1) and (2.2), we may obtain the Helmholtz equation for the scalar potential ϕ and the Maxwell equation for the vector potential ψ , respectively:

$$\Delta \phi + \kappa_n^2 \phi = 0$$
, **curlcurl** $\psi - \kappa_s^2 \psi = 0$.

In addition, ϕ and ψ are required to satisfy the Sommerfeld and the Silver-Müller radiation conditions, respectively:

$$\lim_{\rho \to \infty} \rho(\partial_{\rho} \phi - i\kappa_{\mathfrak{p}} \phi) = 0, \quad \lim_{\rho \to \infty} \rho(\mathbf{curl} \psi \times \hat{x} - i\kappa_{\mathfrak{s}} \psi) = 0, \quad \rho = |x|.$$

It follows from the Helmholtz decomposition and boundary condition on Γ_{D} that

$$\mathbf{v} = \nabla \phi + \mathbf{curl} \psi = -\mathbf{u}^i$$
.

Taking the dot product and the cross product of the above equation with ν , respectively, we get

$$\partial_{\nu}\phi + \nu \cdot \mathbf{curl}\psi = f_1, \quad \nu \times \nabla \phi + \nu \times \mathbf{curl}\psi = f_2,$$
 (2.3)

where

$$f_1 := -\nu \cdot \mathbf{u}^i, \quad \mathbf{f}_2 := -\nu \times \mathbf{u}^i.$$

In summary, the scalar potential function ϕ and the vector potential function ψ satisfy the coupled boundary value problem

$$\begin{cases} \Delta \phi + \kappa_{\mathfrak{p}}^{2} \phi = 0, & \mathbf{curlcurl} \psi - \kappa_{\mathfrak{s}}^{2} \psi = 0 & \text{in } \mathbb{R}^{3} \setminus \overline{D}, \\ \partial_{\nu} \phi + \nu \cdot \mathbf{curl} \psi = f_{1} & \nu \times \nabla \phi + \nu \times \mathbf{curl} \psi = f_{2} & \text{on } \Gamma_{D}, \\ \lim_{\rho \to \infty} \rho (\partial_{\rho} \phi - i \kappa_{\mathfrak{p}} \phi) = 0, & \lim_{\rho \to \infty} \rho (\mathbf{curl} \psi \times \hat{\mathbf{x}} - i \kappa_{\mathfrak{s}} \psi) = 0, & \rho = |\mathbf{x}|. \end{cases}$$

$$(2.4)$$

The following result concerns the uniqueness of the boundary value problem (2.4).

Theorem 2.1. The coupled boundary value problem (2.4) has at most one solution for $\kappa_{\mathfrak{p}} > 0$ and $\kappa_{\mathfrak{s}} > 0$.

Proof. It suffices to show that $\phi = 0$ and $\psi = 0$ in $\mathbb{R}^3 \setminus \overline{D}$ when $f_1 = 0$, $f_2 = 0$. Let B_R be a ball with radius R > 0 such that $D \subset B_R$ and Γ_B be the boundary of B_R . Denote by Ω the bounded domain $\Omega = B_R \setminus \overline{D}$ enclosed by Γ_D and Γ_B . Using the first Green's theorem [6, (2.2) and (6.2)] and noting $\nabla \cdot \psi = 0$, we have

$$\int_{\Gamma_B} \phi \partial_{\nu} \bar{\phi} \, ds = \int_{\Omega} \left(\phi \Delta \bar{\phi} + \nabla \phi \cdot \nabla \bar{\phi} \right) dx + \int_{\Gamma_D} \phi \partial_{\nu} \bar{\phi} \, ds$$
$$= \int_{\Omega} \left(-\kappa_{\mathfrak{p}}^2 |\phi|^2 + |\nabla \phi|^2 \right) dx + \int_{\Gamma_D} \phi \partial_{\nu} \bar{\phi} \, ds$$

and

$$\begin{split} \int\limits_{\Gamma_B} \left(\mathbf{curl} \bar{\boldsymbol{\psi}} \times \hat{\boldsymbol{x}} \right) \cdot \boldsymbol{\psi} \, \mathrm{d}\boldsymbol{s} &= \int\limits_{\Gamma_B} \left(\hat{\boldsymbol{x}} \times \boldsymbol{\psi} \right) \cdot \mathbf{curl} \bar{\boldsymbol{\psi}} \, \mathrm{d}\boldsymbol{s} \\ &= \int\limits_{\Omega} \left(\boldsymbol{\psi} \cdot \Delta \bar{\boldsymbol{\psi}} + \mathbf{curl} \boldsymbol{\psi} \cdot \mathbf{curl} \bar{\boldsymbol{\psi}} \right) \mathrm{d}\boldsymbol{x} + \int\limits_{\Gamma_D} \left(\boldsymbol{v} \times \boldsymbol{\psi} \right) \cdot \mathbf{curl} \bar{\boldsymbol{\psi}} \, \mathrm{d}\boldsymbol{s} \\ &= \int\limits_{\Omega} \left(-\kappa_{\mathfrak{s}}^2 |\boldsymbol{\psi}|^2 + |\mathbf{curl} \boldsymbol{\psi}|^2 \right) \mathrm{d}\boldsymbol{x} + \int\limits_{\Gamma_D} \left(\mathbf{curl} \bar{\boldsymbol{\psi}} \times \boldsymbol{v} \right) \cdot \boldsymbol{\psi} \, \mathrm{d}\boldsymbol{s}. \end{split}$$

Using the boundary condition (2.3), the relation between the gradient and the surface gradient

$$\nabla \varphi = \mathbf{Grad} \varphi + \nu \partial_{\nu} \varphi$$
,

and the identity (cf. [6, Page 204])

$$\int_{\Gamma_D} \varphi(\nu \cdot \mathbf{curl} \psi) \, \mathrm{d}s = \int_{\Gamma_D} \mathbf{Grad} \varphi \cdot (\nu \times \psi) \, \mathrm{d}s,$$

we obtain

$$\Im \int_{\Gamma_{D}} \left(\phi \partial_{\nu} \bar{\phi} + (\mathbf{curl} \bar{\psi} \times \nu) \cdot \psi \right) ds$$

$$= \Im \int_{\Gamma_{D}} \left(-\phi (\mathbf{curl} \bar{\psi} \cdot \nu) - (\nabla \bar{\phi} \times \nu) \cdot \psi \right) ds$$

$$= -\Im \int_{\Gamma_{D}} \left(\mathbf{Grad} \phi \cdot (\nu \times \bar{\psi}) + \mathbf{Grad} \bar{\phi} \cdot (\nu \times \psi) \right) ds = 0.$$
(2.5)

It follows from the radiation conditions (2.4) that

$$\int_{\Gamma_{B}} \left(|\partial_{\nu} \phi|^{2} + \kappa_{\mathfrak{p}}^{2} |\phi|^{2} + 2\kappa_{\mathfrak{p}} \Im(\phi \partial_{\nu} \bar{\phi}) \right) ds = \int_{\Gamma_{B}} |\partial_{\nu} \phi - i\kappa_{\mathfrak{p}} \phi|^{2} ds \to 0$$
(2.6)

and

$$\int_{\Gamma_{B}} \left(|\mathbf{curl}\psi \times \hat{x}|^{2} + \kappa_{\mathfrak{s}}^{2} |\psi|^{2} + 2\kappa_{\mathfrak{s}} \Im((\mathbf{curl}\bar{\psi} \times \hat{x}) \cdot \psi) \right) ds$$

$$= \int_{\Gamma_{B}} |\mathbf{curl}\psi \times \hat{x} - i\kappa_{\mathfrak{s}}\psi|^{2} ds \to 0$$
(2.7)

as $R \to \infty$. Since $\kappa_{\mathfrak{p}} > 0$ and $\kappa_{\mathfrak{s}} > 0$, it follows from (2.5)–(2.7) that

$$\lim_{R\to\infty}\int\limits_{\Gamma_B}\left(\frac{1}{\kappa_{\mathfrak{p}}}|\partial_{\nu}\phi|^2+\kappa_{\mathfrak{p}}|\phi|^2+\frac{1}{\kappa_{\mathfrak{s}}}|\mathbf{curl}\psi\times\hat{x}|^2+\kappa_{\mathfrak{s}}|\psi|^2\right)\mathrm{d}s=0.$$

We have from Rellich's lemma that $\phi = 0$ and $\psi = 0$ in $\mathbb{R}^3 \setminus \overline{D}$, which completes the proof. \Box

It is known that a radiating solution of (2.1) has the asymptotic behavior of the form

$$\boldsymbol{\nu}(x) = \frac{e^{\mathrm{i}\kappa_{\mathfrak{p}}|x|}}{|x|} \boldsymbol{\nu}_{\mathfrak{p}}^{\infty}(\hat{x}) + \frac{e^{\mathrm{i}\kappa_{\mathfrak{s}}|x|}}{|x|} \boldsymbol{\nu}_{\mathfrak{s}}^{\infty}(\hat{x}) + \mathcal{O}\left(\frac{1}{|x|^2}\right), \quad |x| \to \infty$$

uniformly in all directions $\hat{x} := x/|x|$, where $\boldsymbol{v}_{\mathfrak{p}}^{\infty}$ and $\boldsymbol{v}_{\mathfrak{s}}^{\infty}$, defined on the unit sphere $\mathbb{S}^2 = \{\hat{x} \in \mathbb{R}^3 : |\hat{x}| = 1\}$, are called the compressional and shear far-field patterns of \boldsymbol{v} , respectively.

Remark 2.2. By extending the result [9, Theorem 3.1] to three dimensions and using [6, Theorem 6.9], we can establish the relationship between the far-field pattern of the compressional wave \mathbf{v}_p or the shear wave \mathbf{v}_s and the far-field pattern of the scalar potential ϕ or the vector potential ψ , i.e.,

$$\mathbf{v}_{\mathfrak{p}}^{\infty}(\hat{x}) = i\kappa_{\mathfrak{p}}\phi_{\infty}(\hat{x})\hat{x}, \quad \mathbf{v}_{\mathfrak{s}}^{\infty}(\hat{x}) = i\kappa_{\mathfrak{s}}\hat{x} \times \psi_{\infty},$$
 (2.8)

where the complex-valued functions $\phi_{\infty}(\hat{x})$ and $\psi_{\infty}(\hat{x})$ are the far-field patterns corresponding to ϕ and ψ , respectively. Therefore, in view of (2.2) and (2.8), we can obtain the compressional and shear wave components $v_{\mathfrak{p}}$, $v_{\mathfrak{s}}$ and the corresponding far-field patterns $v_{\mathfrak{p}}^{\infty}$, $v_{\mathfrak{s}}^{\infty}$ by solving the coupled boundary value problem (2.4).

3. Boundary integral equations

In this section, we deduce the coupled system of boundary integral equations for solving the boundary value problem (2.4).

Define a vector potential

$$\mathbf{A}\mathbf{g}(x) := \int_{\Gamma_D} \Phi(x, y; \kappa) \mathbf{g}(y) \, \mathrm{d}s(y), \quad x \in \mathbb{R}^3 \setminus \Gamma_D,$$

where ${\bf g}$ is a continuous tangential vector function on Γ_D and

$$\Phi(x, y; \kappa) = \frac{1}{4\pi} \frac{e^{i\kappa|x-y|}}{|x-y|}, \quad x \neq y$$
(3.1)

is the fundamental solution to the three-dimensional Helmholtz equation. Using [6, Theorem 6.13], we have the jump relation

$$\mathbf{curl} \mathbf{A}_{\pm} \mathbf{g}(x) = \int_{\Gamma_0} \nabla_{\mathbf{x}} \Phi(\mathbf{x}, \mathbf{y}; \kappa) \times \mathbf{g}(\mathbf{y}) \, \mathrm{d}s(\mathbf{y}) \mp \frac{1}{2} \nu(\mathbf{x}) \times \mathbf{g}(\mathbf{x}), \tag{3.2}$$

where

$$\operatorname{curl} \mathbf{A}_{\pm} \mathbf{g}(\mathbf{x}) := \lim_{h \to +0} \operatorname{curl} \mathbf{A} \mathbf{g}(\mathbf{x} \pm h \nu(\mathbf{x})).$$

Meanwhile, we have from the Maxwell equation that

$$(\operatorname{curlcurl} A \mathbf{g})_{+}(x) = \kappa^{2} (\operatorname{curl} A \mathbf{g})_{+}(x).$$

We represent the solutions of (2.4) by

$$\begin{cases} \phi(x) &= \int_{\Gamma_D} \Phi(x, y; \kappa_{\mathfrak{p}}) g_1(y) \, \mathrm{d}s(y), \\ \psi(x) &= \frac{1}{\kappa^2} \mathbf{curlcurl} \int_{\Gamma_D} \Phi(x, y; \kappa_{\mathfrak{s}}) \mathbf{g}_2(y) \, \mathrm{d}s(y), \end{cases} \quad x \in \mathbb{R}^3 \setminus \Gamma_D,$$
(3.3)

where g_1 is a scalar density function and g_2 is a tangential vector density function satisfying $g_2 \cdot \nu = 0$. It can be verified from simple calculations that the corresponding far-field patterns can be represented as follows

$$\begin{cases} \phi_{\infty}(\hat{x}) &= \frac{1}{4\pi} \int_{\Gamma_D} e^{-i\kappa_{\mathfrak{p}}\hat{x}\cdot y} g_1(y) \, \mathrm{d}s(y), \\ \psi_{\infty}(\hat{x}) &= \frac{1}{4\pi} \hat{x} \times \int_{\Gamma_D} \mathbf{g}_2(y) \times \hat{x} e^{-i\kappa_{\mathfrak{p}}\hat{x}\cdot y} \, \mathrm{d}s(y). \end{cases}$$
(3.4)

Letting $x \in \mathbb{R}^3 \setminus \overline{D}$ approach the boundary Γ_D in (3.3), using the jump relations (3.2) and

$$\nabla \phi_{\pm}(x) = \int_{\Gamma_{\mathbf{p}}} \nabla_{\mathbf{x}} \Phi(\mathbf{x}, \mathbf{y}; \kappa_{\mathbf{p}}) g_{1}(\mathbf{y}) \, \mathrm{d}s(\mathbf{y}) \mp \frac{1}{2} \nu(\mathbf{x}) g_{1}(\mathbf{x}),$$

and the boundary condition (2.4), we deduce the coupled boundary integral equations for the density functions g_1 and g_2 on Γ_D :

$$\begin{cases}
f_{1}(x) &= -\frac{1}{2}g_{1}(x) + \int_{\Gamma_{D}} \frac{\partial \Phi(x, y; \kappa_{\mathfrak{p}})}{\partial \nu(x)} g_{1}(y) \, \mathrm{d}s(y) \\
&+ \nu(x) \cdot \mathbf{curl}_{x} \int_{\Gamma_{D}} \Phi(x, y; \kappa_{\mathfrak{p}}) g_{2}(y) \, \mathrm{d}s(y), \\
f_{2}(x) &= \nu(x) \times \nabla_{x} \int_{\Gamma_{D}} \Phi(x, y; \kappa_{\mathfrak{p}}) g_{1}(y) \, \mathrm{d}s(y) \\
&+ \nu(x) \times \mathbf{curl}_{x} \int_{\Gamma_{D}} \Phi(x, y; \kappa_{\mathfrak{p}}) g_{2}(y) \, \mathrm{d}s(y) + \frac{1}{2} g_{2}(x).
\end{cases} (3.5)$$

Denote by $C(\Gamma_D)$ the space of all continuous functions on Γ_D , and $C_T(\Gamma_D)$ the space of all continuous tangential vector fields on Γ_D . The following result concerns the uniqueness of the solution to (3.5).

Theorem 3.1. The system of boundary integral equations (3.5) has at most one solution in $C(\Gamma_D) \times C_T(\Gamma_D)$ provided that $\kappa_{\mathfrak{p}}$ is not an interior Dirichlet eigenvalue for the Helmholtz equation in D and $\kappa_{\mathfrak{p}}$ is not an interior Maxwell eigenvalue in D with the homogeneous perfectly conducting boundary condition.

Proof. It suffices to show that $g_1 = 0$ and $g_2 = 0$ if $f_1 = 0$ and $f_2 = 0$. By the uniqueness result in Theorem 2.1, we have

$$\phi(x) = 0$$
, $\psi(x) = 0$, $x \in \mathbb{R}^3 \setminus \overline{D}$.

It follows from the continuity of the single layer potential that $\phi(x) = 0$ for $x \in \Gamma_D$. Since κ_p is not an interior Dirichlet eigenvalue for the Helmholtz equation in D, we get $\phi(x) = 0$ for $x \in D$. Using the jump relation of the derivative of the scalar single-layer potential, we obtain $g_1 = 0$.

Define the integral operator $\mathbf{M}: \mathbf{C}_T(\Gamma_D) \to \mathbf{C}_T(\Gamma_D)$ by

$$(\mathbf{M}\mathbf{g}_2)(x) := 2\nu(x) \times \mathbf{curl} \int_{\Gamma_D} \Phi(x, y; \kappa_{\mathfrak{s}}) \mathbf{g}_2(y) \, \mathrm{d}s(y).$$

Substituting $g_1 = 0$ into the second equation of (3.5), we obtain

$$\mathbf{g}_2(x) + (\mathbf{M}\mathbf{g}_2)(x) = 0.$$

Since κ_s is not an interior Maxwell eigenvalue in D with the perfectly conducting boundary condition $v \times \psi = 0$, we obtain from [5, Theorem 4.23] that $\mathbf{g}_2 = 0$, which completes the proof. \square

Next we introduce the single-layer boundary integral operators S^{σ} , $\sigma = \mathfrak{p}, \mathfrak{s}$ and the normal derivative boundary integral operator K for $g \in C(\Gamma_D)$ and $g \in C_T(\Gamma_D)$ by

$$(S^{\mathfrak{p}}g)(x) = 2 \int_{\Gamma_{D}} \Phi(x, y; \kappa_{\mathfrak{p}}) g(y) \, \mathrm{d}s(y), \quad x \in \Gamma_{D},$$

$$(S^{\mathfrak{s}}g)(x) = 2 \int_{\Gamma_{D}} \Phi(x, y; \kappa_{\mathfrak{s}}) g(y) \, \mathrm{d}s(y), \quad x \in \Gamma_{D},$$

$$(Kg)(x) = 2 \int_{\Gamma_{D}} \frac{\partial \Phi(x, y; \kappa_{\mathfrak{p}})}{\partial \nu(x)} g(y) \, \mathrm{d}s(y), \quad x \in \Gamma_{D},$$

and we also define boundary integral operators N, H and M by

$$(N\mathbf{g})(x) = 2\nu(x) \cdot \mathbf{curl}_{x} \int_{\Gamma_{D}} \Phi(x, y; \kappa_{\mathfrak{s}}) \mathbf{g}(y) \, \mathrm{d}s(y),$$

$$(H\mathbf{g})(x) = 2\nu(x) \times \nabla_{x} \int_{\Gamma_{D}} \Phi(x, y; \kappa_{\mathfrak{p}}) \mathbf{g}(y) \, \mathrm{d}s(y),$$

$$(M\mathbf{g})(x) = 2\nu(x) \times \mathbf{curl}_{x} \int_{\Gamma_{D}} \Phi(x, y; \kappa_{\mathfrak{s}}) \mathbf{g}(y) \, \mathrm{d}s(y),$$

where g and g are the scalar and vector densities, respectively. Then the system (3.5) can be rewritten as

$$\begin{cases}
-g_1 + Kg_1 + N\mathbf{g}_2 = f_1, \\
Hg_1 + \mathbf{g}_2 + M\mathbf{g}_2 = \mathbf{f}_2.
\end{cases}$$
(3.6)

By the decomposition in [10, (2.5)-(2.6)], the kernels of weakly singular integral operators S^{σ} and K can be decomposed into a general form as

$$m(x, y) = \frac{1}{|x - y|} m_1(x, y) + m_2(x, y)$$

with m_i (i = 1, 2) given by

$$m_i(x, y) = m_{i,1}(x, y) + m_{i,2}(x, y) \frac{(x - y) \cdot \nu(y)}{|x - y|^2} + m_{i,3}(x, y) \frac{(x - y) \cdot \nu(x)}{|x - y|^2},$$

where each $m_{i,j}$ $(i=1,2,\ j=1,2,3)$ is infinitely continuously differentiable on $\mathbb{R}^3 \times \mathbb{R}^3$ under the assumption that Γ_D is analytic. Hence, we have for $x \in \Gamma_D$ that

$$(S^{\mathfrak{p}}g)(x) = \int_{\Gamma_{D}} \left(\frac{1}{|x-y|} s_{1}^{\mathfrak{p}}(x,y) + s_{2}^{\mathfrak{p}}(x,y)\right) g(y) \, \mathrm{d}s(y),$$

$$(S^{\mathfrak{s}}g)(x) = \int_{\Gamma_{D}} \left(\frac{1}{|x-y|} s_{1}^{\mathfrak{s}}(x,y) + s_{2}^{\mathfrak{s}}(x,y)\right) g(y) \, \mathrm{d}s(y),$$

$$(Kg)(x) = \int_{\Gamma_{D}} \left(\frac{1}{|x-y|} k_{1}^{\mathfrak{p}}(x,y) + k_{2}^{\mathfrak{p}}(x,y)\right) g(y) \, \mathrm{d}s(y),$$

$$(3.7)$$

where

$$\begin{split} s_1^{\sigma}(x,y) &= \frac{\cos\left(\kappa_{\sigma}\left|x-y\right|\right)}{2\pi}, \quad s_2^{\sigma}(x,y) = \begin{cases} \frac{\mathrm{i}\sin\left(\kappa_{\sigma}\left|x-y\right|\right)}{2\pi\left|x-y\right|}, & x \neq y, \\ \frac{\mathrm{i}\kappa_{\sigma}}{2\pi}, & x = y, \end{cases} \\ k_1^{\mathfrak{p}}(x,y) &= -\frac{\nu(x)\cdot(x-y)}{\left|x-y\right|^2} s_1^{\mathfrak{p}}(x,y) + \mathrm{i}\kappa_{\mathfrak{p}}\nu(x)\cdot(x-y) s_2^{\mathfrak{p}}(x,y), \\ k_2^{\mathfrak{p}}(x,y) &= -\frac{\nu(x)\cdot(x-y)}{\left|x-y\right|^2} \left[s_2^{\mathfrak{p}}(x,y) - \mathrm{i}\kappa_{\mathfrak{p}} s_1^{\mathfrak{p}}(x,y) \right]. \end{split}$$

Similarly, the kernel of weakly singular integral operator M can be decomposed into

$$(M\mathbf{g})(x) = \int_{\Gamma_D} \left(\frac{1}{|x-y|} \mathbf{m}_1(x, y) + \mathbf{m}_2(x, y) \right) \mathbf{g}(y) \, \mathrm{d}s(y)$$

with \mathbf{m}_i (i = 1, 2) being of the form

$$\mathbf{m}_{i}(x, y) = \widetilde{m}_{i,1}(x, y) \frac{(x - y)[\nu(x) - \nu(y)]^{\top}}{|x - y|^{2}} + \widetilde{m}_{i,2}(x, y) \frac{(x - y) \cdot \nu(y)}{|x - y|^{2}} I + \widetilde{m}_{i,3}(x, y),$$

where I is the 3×3 identity matrix, $\widetilde{m}_{2,3}$ is the 3×3 zero matrix, and each $\widetilde{m}_{i,j}$ $(i=1,2,\ j=1,2,3)$ is infinitely continuously differentiable on $\mathbb{R}^3 \times \mathbb{R}^3$. We refer to [12, (2.8)-(2.9)] for the detailed expressions of $\widetilde{m}_{i,j}$.

Since all the boundary operators S^{σ} , K, M have weakly singular kernels, their spectrally accurate discretization can be conveniently obtained by using the spherical harmonics. The details are given in Section 5. However, for the integral operators N and H, their kernels have Cauchy type strong singularities, direct discretization will introduce large errors. In order to design a spectral method for (3.6) via the Galerkin discretization, it is necessary to regularize the singularity of N and H, which is examined in the next section.

4. Spherical parametrization

From now on, we assume that the boundary Γ_D is an isomorphism of a unit sphere, which is a common assumption in the areas of wave scattering and inverse scattering [6]. For two vectors \mathbf{a} , $\mathbf{b} \in \mathbb{R}^3$ and two 3×3 matrices $A = (a_1, a_2, a_3)$, $B = (b_1, b_2, b_3)$, we define

$$\mathbf{a} \otimes \mathbf{b} = \mathbf{a} \mathbf{b}^{\top}, \quad A : B = a_1 \cdot b_1 + a_2 \cdot b_2 + a_3 \cdot b_3$$

Based on a bijective parameterization map $\mathbf{q}: \mathbb{S}^2 \to \Gamma_D$, the boundary integral equations (3.6) can be transformed on the unit sphere \mathbb{S}^2 . By the change of variables $\mathbf{x} = \mathbf{q}(\hat{\mathbf{x}})$, for any integrable function g defined on Γ_D , it holds

$$\int_{\Gamma_D} g(x) \, \mathrm{d}s(x) = \int_{\mathbb{S}^2} g(\boldsymbol{q}(\hat{x})) J_{\boldsymbol{q}}(\hat{x}) \, \mathrm{d}s(\hat{x}),$$

where $I_{\boldsymbol{a}}(\hat{x})$ is the Jacobian of the transformation \boldsymbol{q} .

Denote by (θ, φ) the spherical coordinates of any point $\hat{x} \in \mathbb{S}^2$, i.e.,

$$\hat{x} = p(\theta, \varphi) = (\sin \theta \cos \varphi, \sin \theta \sin \varphi, \cos \theta)^{\top}, \quad \theta \in [0, \pi], \ \varphi \in [0, 2\pi),$$

and the corresponding Jacobian is $J_p(\theta, \varphi) = \sin \theta$. The tangent plane at any point $\hat{x} \in \mathbb{S}^2$ is generated by the unit vectors

$$\mathbf{e}_{\theta} \circ p = \frac{\partial p}{\partial \theta}(\theta, \varphi) = (\cos \theta \cos \varphi, \cos \theta \sin \varphi, -\sin \theta)^{\top},$$

$$\mathbf{e}_{\varphi} \circ p = \frac{1}{\sin \theta} \frac{\partial p}{\partial \varphi}(\theta, \varphi) = (-\sin \varphi, \cos \varphi, 0)^{\top}.$$

The triplet $(\hat{x}, \mathbf{e}_{\theta}, \mathbf{e}_{\varphi})$ forms an orthonormal system. Following the notations in [19,20], we define the tangent vectors on Γ_D by

$$\begin{aligned} \mathbf{t}_{1}(\hat{\mathbf{x}}) &= \frac{\partial \mathbf{q} \circ \mathbf{p}}{\partial \theta} \circ \mathbf{p}^{-1}(\hat{\mathbf{x}}) = [\mathbf{D}_{\mathbb{S}^{2}} \mathbf{q}(\hat{\mathbf{x}})] \mathbf{e}_{\theta}(\hat{\mathbf{x}}), \\ \mathbf{t}_{2}(\hat{\mathbf{x}}) &= \left(\frac{1}{\sin \theta} \frac{\partial \mathbf{q} \circ \mathbf{p}}{\partial \varphi}\right) \circ \mathbf{p}^{-1}(\hat{\mathbf{x}}) = [\mathbf{D}_{\mathbb{S}^{2}} \mathbf{q}(\hat{\mathbf{x}})] \mathbf{e}_{\varphi}(\hat{\mathbf{x}}), \end{aligned}$$

where the matrix $[\mathbf{D}_{\mathbb{S}^2} \mathbf{q}(\hat{x})] = \mathbf{t}_1 \otimes \mathbf{e}_{\theta} + \mathbf{t}_2 \otimes \mathbf{e}_{\varphi}$ maps the tangent plane to \mathbb{S}^2 at the point \hat{x} onto the tangent plane to Γ_D at the point $\mathbf{q}(\hat{x})$, the Jacobian $J_{\mathbf{q}}$ and the normal vector $v \circ \mathbf{q}$ are given by

$$J_{\mathbf{q}} = |\mathbf{t}_1 \times \mathbf{t}_2|, \quad v \circ \mathbf{q} = \frac{\mathbf{t}_1 \times \mathbf{t}_2}{J_{\mathbf{q}}}.$$

By the conclusions in [19,20] and the change of variables $x = \mathbf{q}(\hat{x})$, for any smooth w and $\mathbf{w} = (w_1, w_2, w_3)^{\top}$, we may define the following surface scalar and vector curl operators on Γ_D :

$$(\mathbf{curl}_{\Gamma_D} w) \circ \mathbf{q} = \frac{1}{J_{\mathbf{q}}} [\mathbf{D}_{\mathbb{S}^2} \mathbf{q}(\hat{x})] \mathbf{curl}_{\mathbb{S}^2} (w \circ \mathbf{q}), \tag{4.1}$$

$$(\operatorname{curl}_{\Gamma_D} \boldsymbol{w}) \circ \boldsymbol{q} = -\frac{1}{J_{\boldsymbol{q}}} [\mathbf{D}_{\mathbb{S}^2} \boldsymbol{q}(\hat{\boldsymbol{x}})]^{\top} : \mathbf{curl}_{\mathbb{S}^2} (\boldsymbol{w} \circ \boldsymbol{q}), \tag{4.2}$$

where $\operatorname{curl}_{\mathbb{S}^2}(w \circ q) = (\operatorname{Grad}_{\mathbb{S}^2}(w \circ q)) \times \hat{x}$, and

$$\mathbf{Grad}_{\mathbb{S}^2}(w \circ \mathbf{q}) = \left(\frac{\partial w \circ \mathbf{q} \circ p}{\partial \theta}\right) \circ p^{-1} \mathbf{e}_{\theta} + \left(\frac{1}{\sin \theta} \frac{\partial w \circ \mathbf{q} \circ p}{\partial \varphi}\right) \circ p^{-1} \mathbf{e}_{\varphi}. \tag{4.3}$$

Here $\operatorname{\mathbf{curl}}_{\mathbb{S}^2}(\boldsymbol{w} \circ \boldsymbol{q})$ is a matrix whose j-th column is $\operatorname{\mathbf{curl}}_{\mathbb{S}^2}w_j \circ \boldsymbol{q}$. Using (4.3) and the representation of $\mathbf{D}_{\mathbb{S}^2}\boldsymbol{q}$ and $\operatorname{\mathbf{curl}}_{\mathbb{S}^2}(\boldsymbol{w} \circ \boldsymbol{q})$, we obtain

$$\begin{aligned}
& \left(\left[\mathbf{D}_{\mathbb{S}^{2}} \mathbf{q} \right]^{\top} : \mathbf{curl}_{\mathbb{S}^{2}} (\mathbf{w} \circ \mathbf{q}) \right) \circ p \\
&= \frac{1}{\sin \theta} (\mathbf{t}_{1} \circ p) \cdot \frac{\partial \mathbf{w} \circ \mathbf{q} \circ p}{\partial \varphi} - (\mathbf{t}_{2} \circ p) \cdot \frac{\partial \mathbf{w} \circ \mathbf{q} \circ p}{\partial \theta}.
\end{aligned} \tag{4.4}$$

After the parametrization, the boundary operators S^{σ} , K, M can be equivalently rewritten as:

$$(\mathcal{S}^{\mathfrak{p}}G)(\hat{x}) = \int_{\mathbb{S}^{2}} \left(\frac{1}{|\hat{x} - \hat{y}|} \widetilde{S}_{1}^{\mathfrak{p}}(\hat{x}, \hat{y}) + \widetilde{S}_{2}^{\mathfrak{p}}(\hat{x}, \hat{y})\right) G(\hat{y}) \, \mathrm{d}s(\hat{y}),$$

$$(\mathcal{S}^{\mathfrak{s}}G)(\hat{x}) = \int_{\mathbb{S}^{2}} \left(\frac{1}{|\hat{x} - \hat{y}|} \widetilde{S}_{1}^{\mathfrak{s}}(\hat{x}, \hat{y}) + \widetilde{S}_{2}^{\mathfrak{s}}(\hat{x}, \hat{y})\right) G(\hat{y}) \, \mathrm{d}s(\hat{y}),$$

$$(\mathcal{K}G)(\hat{x}) = \int_{\mathbb{S}^{2}} \left(\frac{1}{|\hat{x} - \hat{y}|} \widetilde{K}_{1}(\hat{x}, \hat{y}) + \widetilde{K}_{2}(\hat{x}, \hat{y})\right) G(\hat{y}) \, \mathrm{d}s(\hat{y}),$$

$$(\mathcal{M}G)(\hat{x}) = \int_{\mathbb{S}^{2}} \left(\frac{1}{|\hat{x} - \hat{y}|} \widetilde{M}_{1}(\hat{x}, \hat{y}) + \widetilde{M}_{2}(\hat{x}, \hat{y})\right) G(\hat{y}) \, \mathrm{d}s(\hat{y}),$$

$$(\mathcal{M}G)(\hat{x}) = \int_{\mathbb{S}^{2}} \left(\frac{1}{|\hat{x} - \hat{y}|} \widetilde{M}_{1}(\hat{x}, \hat{y}) + \widetilde{M}_{2}(\hat{x}, \hat{y})\right) G(\hat{y}) \, \mathrm{d}s(\hat{y}),$$

where $G = g \circ q$, $G = g \circ q$, and the kernels for $\sigma = \mathfrak{p}$ or \mathfrak{s} are given by

$$\begin{split} R(\hat{x},\,\hat{y}) &= \frac{|\hat{x} - \hat{y}|}{|\mathbf{q}(\hat{x}) - \mathbf{q}(\hat{y})|}, \\ \widetilde{S}_{1}^{\sigma}(\hat{x},\,\hat{y}) &= R(\hat{x},\,\hat{y})s_{1}^{\sigma}(\mathbf{q}(\hat{x}),\,\mathbf{q}(\hat{y}))J_{\mathbf{q}}(\hat{y}), \\ \widetilde{K}_{1}(\hat{x},\,\hat{y}) &= R(\hat{x},\,\hat{y})k_{1}^{p}(\mathbf{q}(\hat{x}),\,\mathbf{q}(\hat{y}))J_{\mathbf{q}}(\hat{y})J_{\mathbf{q}}(\hat{x}), \\ \widetilde{M}_{1}(\hat{x},\,\hat{y}) &= R(\hat{x},\,\hat{y})m_{1}(\mathbf{q}(\hat{x}),\,\mathbf{q}(\hat{y}))J_{\mathbf{q}}(\hat{y})J_{\mathbf{q}}(\hat{x}), \\ \widetilde{M}_{2}(\hat{x},\,\hat{y}) &= R_{2}^{p}(\mathbf{q}(\hat{x}),\,\mathbf{q}(\hat{y}))J_{\mathbf{q}}(\hat{y})J_{\mathbf{q}}(\hat{x}), \\ \widetilde{M}_{2}(\hat{x},\,\hat{y}) &= m_{2}(\mathbf{q}(\hat{x}),\,\mathbf{q}(\hat{y}))J_{\mathbf{q}}(\hat{y})J_{\mathbf{q}}(\hat{x}). \end{split}$$

As we mentioned before, due to the strong singularities in N and H, it is difficult to achieve high order accuracy by the direct discretization of N and H. As a regularization technique, the following two theorems describe the Galerkin approach by transforming the singularities of N and H to the test functions.

Theorem 4.1. For any smooth scalar function $\varphi(\hat{x})$ on \mathbb{S}^2 , we have

$$\left(J_{\mathbf{q}}(N\mathbf{g}) \circ \mathbf{q}, \varphi \right) = \left(\mathcal{S}^{\mathfrak{s}} \mathbf{G}, [\mathbf{D}_{\mathbb{S}^{2}} \mathbf{q}] \mathbf{curl}_{\mathbb{S}^{2}} \varphi \right), \tag{4.6}$$

where (\cdot, \cdot) is the L_2 inner product on \mathbb{S}^2 .

Proof. Using [22, Theorem 2.5.20], we have

$$N\mathbf{g}(x) = \operatorname{curl}_{\Gamma_D} \left((\nu(x) \times (S^{\mathfrak{s}}\mathbf{g})(x)) \times \nu(x) \right), \quad x \in \Gamma_D.$$

$$(4.7)$$

It follows from Stokes' theorem that

$$\int_{\Gamma_D} \boldsymbol{w} \cdot \mathbf{curl}_{\Gamma_D} u \, \mathrm{d}s = \int_{\Gamma_D} u \, \mathrm{curl}_{\Gamma_D} \boldsymbol{w} \, \mathrm{d}s,\tag{4.8}$$

for any differentiable scalar function u and tangential vector function w on Γ_D . Combining (4.1) and (4.7)–(4.8) gives

$$\begin{split} \left(\int_{\boldsymbol{q}} (N\boldsymbol{g}) \circ \boldsymbol{q}, \varphi \right) &= \int\limits_{\mathbb{S}^{2}} J_{\boldsymbol{q}}(\hat{\boldsymbol{x}}) (N\boldsymbol{g}) \circ \boldsymbol{q}(\hat{\boldsymbol{x}}) \overline{\varphi(\hat{\boldsymbol{x}})} \, \mathrm{d}s(\hat{\boldsymbol{x}}) \\ &= \int\limits_{\Gamma_{D}} (N\boldsymbol{g})(\boldsymbol{x}) \overline{\varphi \circ \boldsymbol{q}^{-1}(\boldsymbol{x})} \, \mathrm{d}s(\boldsymbol{x}) \\ &= \int\limits_{\Gamma_{D}} \overline{\varphi \circ \boldsymbol{q}^{-1}(\boldsymbol{x})} \, \mathrm{curl}_{\Gamma_{D}} \left((\boldsymbol{v}(\boldsymbol{x}) \times (S^{\mathfrak{s}}\boldsymbol{g})(\boldsymbol{x})) \times \boldsymbol{v}(\boldsymbol{x}) \right) \, \mathrm{d}s(\boldsymbol{x}) \\ &= \int\limits_{\Gamma_{D}} \left((\boldsymbol{v}(\boldsymbol{x}) \times (S^{\mathfrak{s}}\boldsymbol{g})(\boldsymbol{x})) \times \boldsymbol{v}(\boldsymbol{x}) \right) \cdot \overline{\mathbf{curl}_{\Gamma_{D}} \varphi \circ \boldsymbol{q}^{-1}(\boldsymbol{x})} \, \mathrm{d}s(\boldsymbol{x}) \\ &= \int\limits_{\Gamma_{D}} (S^{\mathfrak{s}}\boldsymbol{g})(\boldsymbol{x}) \cdot \overline{\mathbf{curl}_{\Gamma_{D}} \varphi \circ \boldsymbol{q}^{-1}(\boldsymbol{x})} \, \mathrm{d}s(\boldsymbol{x}) \\ &= \int\limits_{\Gamma_{D}} (S^{\mathfrak{s}}\boldsymbol{G})(\hat{\boldsymbol{x}}) \cdot \overline{[\mathbf{D}_{\mathbb{S}^{2}}\boldsymbol{q}(\hat{\boldsymbol{x}})] \mathbf{curl}_{\mathbb{S}^{2}} \varphi(\hat{\boldsymbol{x}})} \, \mathrm{d}s(\hat{\boldsymbol{x}}), \end{split}$$

which completes the proof. \Box

Theorem 4.2. For any smooth vector function $\varphi(\hat{x})$ on \mathbb{S}^2 , we have

$$(J_{\mathbf{q}}(Hg) \circ \mathbf{q}, \boldsymbol{\varphi}) = (S^{\mathfrak{p}}G, [\mathbf{D}_{\mathbb{S}^2}\mathbf{q}]^{\top} : \mathbf{curl}_{\mathbb{S}^2}\boldsymbol{\varphi}). \tag{4.9}$$

Proof. For $x \in \Gamma_D$, since $\nabla w = \mathbf{Grad}_{\Gamma_D} w + \nu \partial_{\nu} w$, we have

$$(Hg)(x) = 2\nu(x) \times \mathbf{Grad}_{\Gamma_D} \int_{\Gamma_D} \Phi(x, y; \kappa_{\mathfrak{p}}) g(y) \, \mathrm{d}s(y) = -\mathbf{curl}_{\Gamma_D} (S^{\mathfrak{p}} g)(x). \tag{4.10}$$

Using (4.2), (4.10) and Stokes' theorem (4.8), we obtain

$$\left(\int_{\mathbf{q}} (Hg) \circ \mathbf{q}, \boldsymbol{\varphi} \right) = \int_{\mathbb{S}^{2}} \int_{\mathbf{q}} (\hat{x}) [(Hg) \circ \mathbf{q}(\hat{x})] \cdot \overline{\boldsymbol{\varphi}(\hat{x})} \, \mathrm{d}s(\hat{x})
= \int_{\Gamma_{D}} (Hg)(x) \cdot \overline{\boldsymbol{\varphi} \circ \mathbf{q}^{-1}(x)} \, \mathrm{d}s(x)
= -\int_{\Gamma_{D}} \mathbf{curl}_{\Gamma_{D}} (S^{\mathfrak{p}}g)(x) \cdot \overline{\boldsymbol{\varphi} \circ \mathbf{q}^{-1}(x)} \, \mathrm{d}s(x)$$

$$= -\int_{\Gamma_D} (S^{\mathfrak{p}}g)(x) \overline{\operatorname{curl}_{\Gamma_D} \varphi \circ q^{-1}(x)} \, \mathrm{d}s(x)$$

$$= \int_{\mathbb{S}^2} (S^{\mathfrak{p}}G)(\hat{x}) \overline{[\mathbf{D}_{\mathbb{S}^2}q]^{\top} : \mathbf{curl}_{\mathbb{S}^2} \varphi} \, \mathrm{d}s(\hat{x}),$$

which completes the proof. \Box

5. Numerical discretization

Motivated by [10], we propose a fully discrete Galerkin type method with spectral accuracy. To approximate the scalar density functions on the unit sphere, we choose $(n + 1)^2$ -dimensional space of all spherical harmonics of degree less than or equal to n, denoted by

$$X_n = \text{span}\{Y_{l,i}(\hat{x}) : 0 \le l \le n, |j| \le l\},\$$

where

$$Y_{l,j}(\hat{x}) = Y_{l,j}(p(\theta,\varphi)) = c_l^j P_l^{|j|}(\cos\theta) e^{ij\varphi}, \quad c_l^j = (-1)^{(j+|j|)/2} \sqrt{\frac{2l+1}{4\pi} \frac{(l-|j|)!}{(l+|j|)!}}$$

for $l = 0, 1, 2, \dots, |j| \le l$ form a complete orthonormal system in $L^2(\mathbb{S}^2)$, and $P_l^{|j|}$ denote the associated Legendre functions of degree l with order |j|. Analogously to [11], we introduce

$$X_n = \text{span}\{Y_{l,i,k}(\hat{x}): Y_{l,i,k} = Y_{l,i}e_k, 0 \le l \le n, |j| \le l, k = 1, 2, 3\},$$

where e_k denotes the kth Euclidean vector.

It follows from [20] and (4.3) that the tangential gradient of the spherical harmonics is given by

$$\begin{aligned} & \mathbf{Grad}_{\mathbb{S}^2} Y_{l,j}(p(\theta,\varphi)) \\ &= \begin{cases} c_l^j \Big(\frac{\partial P_l^{|j|}(\cos\theta)}{\partial \theta} \mathrm{e}^{\mathrm{i}j\varphi} \boldsymbol{e}_{\theta} \circ p + \mathrm{i}j P_l^{|j|}(\cos\theta) \mathrm{e}^{\mathrm{i}j\varphi} \frac{\boldsymbol{e}_{\varphi} \circ p}{\sin\theta} \Big), & \sin\theta \neq 0, \\ \sqrt{\frac{2l+1}{4\pi}} \sqrt{l(l+1)} \Big(\frac{(\cos\theta)^l}{2} \boldsymbol{e}_{\theta} \circ p + \mathrm{i}j \frac{(\cos\theta)^{l+1}}{2} \boldsymbol{e}_{\varphi} \circ p \Big), & \sin\theta = 0, |j| = 1, \\ (0,0,0)^\top, & \sin\theta = 0, |j| \neq 1, \end{cases} \end{aligned}$$

where

$$\frac{\partial P_l^{|j|}(\cos \theta)}{\partial \theta} = -\frac{(l+1)\cos \theta}{\sin \theta} P_l^{|j|}(\cos \theta) + \frac{l-|j|+1}{\sin \theta} P_{l+1}^{|j|}(\cos \theta), \quad \sin \theta \neq 0.$$

It is clear to note that $\operatorname{Grad}_{\mathbb{S}^2} Y_{l,j}$ is a tangential vector on \mathbb{S}^2 but may not be a tangential vector on the boundary Γ_D . To approximate the tangential vector density functions on the parametrized surface Γ_D , we choose the following ansatz space [12]:

$$\underline{\mathbb{T}_n} = \operatorname{span} \left\{ \mathbf{Z}_{l,j}^{(\tilde{k})}(\hat{x}) : 1 \le l \le n, \ |j| \le l, \ \tilde{k} = 1, 2 \right\},\,$$

where

$$\begin{split} & \boldsymbol{Z}_{l,j}^{(1)}(\hat{x}) = \frac{1}{\sqrt{l(l+1)}} \mathcal{F}(\hat{x}) \mathbf{Grad}_{\mathbb{S}^2} Y_{l,j}(\hat{x}), \\ & \boldsymbol{Z}_{l,j}^{(2)}(\hat{x}) = \frac{1}{\sqrt{l(l+1)}} \mathcal{F}(\hat{x}) \hat{x} \times \mathbf{Grad}_{\mathbb{S}^2} Y_{l,j}(\hat{x}), \end{split}$$

and $\mathbf{Z}_{0,0}^{(1)} = \mathbf{Z}_{0,0}^{(2)} = 0$. Here $\mathcal{F}(\hat{x})$ is an orthogonal transformation that transforms tangential functions on \mathbb{S}^2 to tangential functions on Γ_D . More explicitly, for a given vector $\mathbf{y} \in \mathbb{C}^3$, $\mathcal{F}(\hat{x})$ is given by

$$\mathcal{F}(\hat{x})\mathbf{y} = \cos\psi\mathbf{y} + [\hat{x} \times \nu \circ \mathbf{q}] \times \mathbf{y} + \frac{1}{1 + \cos\psi}[\hat{x} \times \nu \circ \mathbf{q}]^{\top}\mathbf{y}[\hat{x} \times \nu \circ \mathbf{q}],$$

where ψ is the angle between \hat{x} and $\nu \circ q(\hat{x})$. More properties on $\mathcal{F}(\hat{x})$ can be found in [12].

Let $-1 < z_1 < z_2 < \cdots < z_{n+1} < 1$ denote the zeros of the Legendre polynomial P_{n+1} , and consider the Gaussian product rule for the numerical integration of a continuous function over \mathbb{S}^2 :

$$\int_{\mathbb{R}^2} f(\hat{\mathbf{y}}) \, \mathrm{d}\mathbf{s}(\hat{\mathbf{y}}) \approx \sum_{r=0}^{2n+1} \sum_{s=1}^{n+1} \mu_r \nu_s f(p(\theta_s, \varphi_r)) := Q_n(f),$$

where the weights μ_r and ν_s are given by

$$\mu_r = \frac{\pi}{n+1}, \quad \nu_s = \frac{2(1-z_s^2)}{[(n+1)P_n(z_s)]^2},$$

and the quadrature knots θ_s and φ_r are

$$\theta_{\rm S} = \arccos z_{\rm S}, \qquad \varphi_{\rm r} = \frac{r\pi}{n+1}.$$

Let $C(\mathbb{S}^2)$ be the space of continuous functions on \mathbb{S}^2 and $\mathbf{C}(\mathbb{S}^2)$ the vector function space on \mathbb{S}^2 with each component in $C(\mathbb{S}^2)$. Define the discrete orthogonal projection operators $\mathcal{L}_n^{\mathfrak{p}}: C(\mathbb{S}^2) \to X_n$ and $\mathcal{L}_n^{\mathfrak{s}}: \mathbf{C}(\mathbb{S}^2) \to X_n$ by

$$\mathcal{L}_n^{\mathfrak{p}}\psi = \sum_{l=0}^n \sum_{|j|< l} (\psi, Y_{l,j})_n Y_{l,j}, \quad \psi \in C(\mathbb{S}^2),$$

$$\mathcal{L}_n^{\mathfrak{s}} \Psi = \sum_{l=0}^n \sum_{|i| < l} \sum_{k=1}^3 (\Psi, \mathbf{Y}_{l,j,k})_n \mathbf{Y}_{l,j,k}, \quad \Psi \in \mathbf{C}(\mathbb{S}^2),$$

where we have set $(\psi, Y_{l,j})_n = Q_n(\psi \overline{Y}_{l,j})$ and the discrete inner product on \mathbb{S}^2 for two vector functions \mathbf{G} and \mathbf{Z} is denoted by $(\mathbf{G}, \mathbf{Z})_n = Q_n(\overline{\mathbf{Z}}^{\top}\mathbf{G})$.

Now we describe the approximation in details for (4.6) and (4.9). Following [10,12], we split the kernels in (4.5) into a weakly singular part and an analytic part. In order to accurately integrate the weakly singular part, an orthogonal transformation is introduced on \mathbb{S}^2 and the singularity is transferred to the north pole $\hat{n} = (0,0,1)$. In particular, if $\hat{x} = p(\theta,\varphi)$, the orthogonal transformation is defined by $T_{\hat{x}} := D_P(\varphi)D_Q(\theta)D_P(-\varphi)$, i.e., $T_{\hat{x}}\hat{x} = \hat{n}$, where

$$D_P(\psi) = \begin{bmatrix} \cos \psi & -\sin \psi & 0 \\ \sin \psi & \cos \psi & 0 \\ 0 & 0 & 1 \end{bmatrix}, \quad D_Q(\psi) = \begin{bmatrix} \cos \psi & 0 & -\sin \psi \\ 0 & 1 & 0 \\ \sin \psi & 0 & \cos \psi \end{bmatrix}.$$

Define the linear and bilinear transformations by

$$T_{\hat{\chi}}\Psi(\hat{z}) := \Psi(T_{\hat{\chi}}^{-1}\hat{z}), \quad T_{\hat{\chi}}\Psi(\hat{z}_1,\hat{z}_2) := \Psi(T_{\hat{\chi}}^{-1}\hat{z}_1,T_{\hat{\chi}}^{-1}\hat{z}_2).$$

Using the fact that

$$|\hat{x} - \hat{y}| = |T_{\hat{x}}^{-1}(\hat{n} - \hat{z})| = |\hat{n} - \hat{z}|,$$

we can write \mathcal{S}^{σ} in (4.5) as

$$(\mathcal{S}^{\sigma}\widetilde{G}_{\sigma})(\hat{x}) = \int_{\mathbb{S}^{2}} \left(\frac{1}{|\hat{n} - \hat{z}|} T_{\hat{x}} \widetilde{S}_{1}^{\sigma}(\hat{n}, \hat{z}) + T_{\hat{x}} \widetilde{S}_{2}^{\sigma}(\hat{n}, \hat{z}) \right) T_{\hat{x}} \widetilde{G}_{\sigma}(\hat{z}) \, \mathrm{d}s(\hat{z})$$

for $\sigma = \mathfrak{p}, \mathfrak{s}$, where $\widetilde{G}_{\mathfrak{p}} = g_1 \circ \boldsymbol{q}$ and $\widetilde{G}_{\mathfrak{s}} = \boldsymbol{g}_2 \circ \boldsymbol{q}$. Then, by using

$$\int_{\mathbb{S}^2} \frac{1}{|\hat{x} - \hat{y}|} Y_{l,j}(\hat{y}) \, ds(\hat{y}) = \frac{4\pi}{2l+1} Y_{l,j}(\hat{x}), \quad \hat{x} \in \mathbb{S}^2$$

and the addition theorem

$$\sum_{i=-l}^{l} Y_{l,j}(\hat{x}) \overline{Y_{l,j}(\hat{y})} = \frac{2l+1}{4\pi} P_l(\cos \bar{\theta}),$$

where $\bar{\theta}$ denotes the angle between \hat{x} and \hat{y} , the approximation $S_{n'}^{\sigma}$ for the operators S^{σ} can be represented as

$$\begin{split} (\mathcal{S}_{n'}^{\sigma}\widetilde{\mathbf{G}}_{\sigma})(\hat{\mathbf{x}}) &:= \int\limits_{\mathbb{S}^{2}} \frac{1}{|\hat{\mathbf{n}} - \hat{\mathbf{z}}|} \mathcal{L}_{n'}^{\sigma} \left\{ T_{\hat{\mathbf{x}}} \widetilde{\mathbf{S}}_{1}^{\sigma}(\hat{\mathbf{n}}, \hat{\mathbf{z}}) T_{\hat{\mathbf{x}}} \widetilde{\mathbf{G}}_{\sigma}(\hat{\mathbf{z}}) \right\} \mathrm{d}\mathbf{s}(\hat{\mathbf{z}}) + \int\limits_{\mathbb{S}^{2}} \mathcal{L}_{n'}^{\sigma} \left\{ T_{\hat{\mathbf{x}}} \widetilde{\mathbf{S}}_{2}^{\sigma}(\hat{\mathbf{n}}, \hat{\mathbf{z}}) T_{\hat{\mathbf{x}}} \widetilde{\mathbf{G}}_{\sigma}(\hat{\mathbf{z}}) \right\} \mathrm{d}\mathbf{s}(\hat{\mathbf{z}}) \\ &= \sum_{r'=0}^{2n'+1} \sum_{s'=1}^{n'} \xi_{r'} \eta_{s'} \left[\alpha_{s'}^{n'} T_{\hat{\mathbf{x}}} \widetilde{\mathbf{S}}_{1}^{\sigma}(\hat{\mathbf{n}}, \hat{\mathbf{y}}_{r's'}) + T_{\hat{\mathbf{x}}} \widetilde{\mathbf{S}}_{2}^{\sigma}(\hat{\mathbf{n}}, \hat{\mathbf{y}}_{r's'}) \right] T_{\hat{\mathbf{x}}} \widetilde{\mathbf{G}}_{\sigma}(\hat{\mathbf{y}}_{r's'}). \end{split}$$

Here $\alpha_{s'}^{n'} := \sum_{l=0}^{n'} P_l(\hat{n} \cdot \hat{y}_{r's'})$, $\xi_{r'} = \mu_{r'}$ and $\eta_{s'} = \nu_{s'}$. In view of Theorems 4.1 and 4.2, the Galerkin method for (3.6) seeks to approximate solutions $\widetilde{G}_{\mathfrak{p}}^n \in X_n$ and $\widetilde{G}_{\mathfrak{s}}^n \in \underline{\mathbb{T}_n}$. which can be written as

$$\widetilde{G}_{\mathfrak{p}}^{n}(\hat{x}) = \sum_{l=0}^{n} \sum_{j=-l}^{l} w_{lj} Y_{l,j}(\hat{x}), \quad \widetilde{G}_{\mathfrak{s}}^{n}(\hat{x}) = \sum_{l=0}^{n} \sum_{j=-l}^{l} \sum_{\tilde{k}-1}^{2} W_{lj\tilde{k}} \mathbf{Z}_{l,j}^{(\tilde{k})}(\hat{x}),$$

and satisfy

$$\begin{cases}
-(J_{\mathbf{q}}\widetilde{G}_{\mathfrak{p}}^{n}, Y_{l',j'})_{n+1} + (\mathcal{K}_{n'}\widetilde{G}_{\mathfrak{p}}^{n}, Y_{l',j'})_{n+1} \\
+(\mathcal{S}_{n'}^{\mathfrak{s}}\widetilde{G}_{\mathfrak{s}}^{n}, [\mathbf{D}_{\mathbb{S}^{2}}\mathbf{q}]\mathbf{curl}_{\mathbb{S}^{2}}Y_{l',j'})_{n+1} = 2(\tilde{f}_{1}J_{\mathbf{q}}, Y_{l',j'})_{n+1}, \\
(\mathcal{S}_{n'}^{\mathfrak{p}}\widetilde{G}_{\mathfrak{p}}^{n}, [\mathbf{D}_{\mathbb{S}^{2}}\mathbf{q}]^{\top} : \mathbf{curl}_{\mathbb{S}^{2}}Z_{l',j'}^{(1)})_{n+1} + (J_{\mathbf{q}}\widetilde{G}_{\mathfrak{s}}^{n}, Z_{l',j'}^{(1)})_{n+1} \\
+(\mathcal{M}_{n'}\widetilde{G}_{\mathfrak{s}}^{n}, \mathbf{Z}_{l',j'}^{(1)})_{n+1} = 2(\tilde{f}_{2}J_{\mathbf{q}}, Z_{l',j'}^{(1)})_{n+1}, \\
(\mathcal{S}_{n'}^{\mathfrak{p}}\widetilde{G}_{\mathfrak{p}}^{n}, [\mathbf{D}_{\mathbb{S}^{2}}\mathbf{q}]^{\top} : \mathbf{curl}_{\mathbb{S}^{2}}Z_{l',j'}^{(2)})_{n+1} + (J_{\mathbf{q}}\widetilde{G}_{\mathfrak{s}}^{n}, Z_{l',j'}^{(2)})_{n+1} \\
+(\mathcal{M}_{n'}\widetilde{G}_{\mathfrak{s}}^{n}, \mathbf{Z}_{l',j'}^{(2)})_{n+1} = 2(\tilde{f}_{2}J_{\mathbf{q}}, \mathbf{Z}_{l',j'}^{(2)})_{n+1}
\end{cases} (5.1)$$

for $l'=0,1,\cdots,n,\ |j'|\leq l',$ where $\tilde{f}_1=f_1\circ \pmb{q},\ \tilde{\pmb{f}}_2=\pmb{f}_2\circ \pmb{q}$ and n'=an+1 with a>1. To assemble the matrix, we denote the corresponding matrix elements in (5.1) by

$$\begin{split} \mathbf{N}_{l'j',lj}^{\tilde{k}} &:= \left(\mathcal{S}_{n'}^{\mathfrak{s}} \mathbf{Z}_{l,j}^{(\tilde{k})}, [\mathbf{D}_{\mathbb{S}^{2}} \boldsymbol{q}] \mathbf{curl}_{\mathbb{S}^{2}} Y_{l',j'}\right)_{n+1}, \quad \tilde{k} = 1, 2, \\ \mathbf{H}_{l'j',lj}^{k'} &:= \left(\mathcal{S}_{n'}^{\mathfrak{p}} Y_{l,j}, [\mathbf{D}_{\mathbb{S}^{2}} \boldsymbol{q}]^{\top} : \mathbf{curl}_{\mathbb{S}^{2}} \mathbf{Z}_{l',j'}^{(k')}\right)_{n+1}, \quad k' = 1, 2, \\ \mathbf{U}_{l'j',lj}^{k',\tilde{k}} &:= \left(J_{\boldsymbol{q}} \mathbf{Z}_{l,j}^{(\tilde{k})}, \mathbf{Z}_{l',j'}^{(k')}\right)_{n+1}, \quad \mathbf{I}_{l'j',lj} := \left(J_{\boldsymbol{q}} Y_{l,j}, Y_{l',j'}\right)_{n+1}, \quad k', \tilde{k} = 1, 2, \\ \mathbf{M}_{l'j',lj}^{k',\tilde{k}} &:= (\mathcal{M}_{n'} \mathbf{Z}_{lj}^{(\tilde{k})}, \mathbf{Z}_{l'j'}^{(k')})_{n+1}, \quad \mathbf{K}_{l'j',lj} := (\mathcal{K}_{n'} Y_{l,j}, Y_{l',j'})_{n+1}, \quad k', \tilde{k} = 1, 2. \end{split}$$

Let us also introduce the following notations

$$\hat{\mathbf{x}}_{rs} = p(\theta_s, \varphi_r), \quad \hat{\mathbf{y}}_{r's'} = p(\Theta_{s'}, \Phi_{r'}), \tag{5.2}$$

$$\hat{y}_{rs}^{r's'} = T_{n(\theta_{s'}, \theta_{s'})}^{-1} p(\Theta_{s'}, \Phi_{r'}) := p(\Lambda_{rs}^{r's'}, \Xi_{rs}^{r's'})$$
(5.3)

with the quadrature knots θ_s , φ_r , $\Theta_{s'}$, $\varphi_{r'}$. Note that $\sin \theta_s \neq 0$ and $\sin \Theta_{s'} \neq 0$ as taking Gaussian quadrature nodes. Since the singularity is transferred to the north pole, we need the representation of rotated spherical harmonics. It follows from standard calculations [11] that

$$Y_{l,j}(\hat{y}_{rs}^{r's'}) = \sum_{\tilde{i}=-l}^{l} F_{s\tilde{l}\tilde{j}j} e^{i(j-\tilde{j})\varphi_r} Y_{l,\tilde{j}}(\hat{y}_{r's'}), \tag{5.4}$$

$$\mathbf{Z}_{l,j}^{(\tilde{k})}(\hat{y}_{rs}^{r's'}) = \mathcal{F}(\hat{y}_{rs}^{r's'}) \sum_{\tilde{i}=-l}^{l} F_{sl\tilde{j}j} e^{i(j-\tilde{j})\varphi_{r}} \sum_{d=1}^{2} \alpha_{l,j}^{(\tilde{k},d)}(\Theta_{s'}) e^{i\tilde{j}\Phi_{r'}} T_{\hat{x}_{rs}}^{-1} \mathbf{v}^{(d)}(\Theta_{s'}, \Phi_{r'}),$$
(5.5)

where

$$F_{sl\tilde{j}j} = e^{i(j-\tilde{j})\pi/2} \sum_{m=-l}^{l} d_{\tilde{j}m}^{(l)}(\pi/2) d_{jm}^{(l)}(\pi/2) e^{im\theta_s},$$

$$\mathbf{v}^{(1)}(\theta, \phi) = (\cos\theta\cos\phi, \cos\theta\sin\phi, -\sin\theta)^T,$$

$$\mathbf{v}^{(2)}(\theta,\phi) = (-\cos\phi,\cos\theta,0)^T$$

$$\alpha_{l,j}^{(1,1)}(\theta) = \alpha_{l,j}^{(2,2)}(\theta) = \frac{1}{\sqrt{l(l+1)}} c_l^j \frac{\partial P_l^{|j|}(\cos \theta)}{\partial \theta},$$

$$\alpha_{l,j}^{(1,2)}(\theta) = \alpha_{l,j}^{(2,1)}(\theta) = \frac{1}{\sqrt{l(l+1)}} c_l^j \frac{ij}{\sin \theta} P_l^{|j|}(\cos \theta).$$

Here

$$d_{jm}^{(l)}(\pi/2) = 2^{j} \sqrt{\frac{(l+j)!(l-j)!}{(l+m)!(l-m)!}} \mathcal{P}_{l+j}^{(m-j,-m-j)}(0),$$

and $\mathcal{P}_{\bar{n}}^{(\alpha,\beta)}$ is the normalized Jacobi polynomial with

$$\mathcal{P}_{\bar{n}}^{(\alpha,\beta)}(0) = 2^{-\bar{n}} \sum_{\bar{t}=0}^{\bar{n}} (-1)^{\bar{t}} \begin{pmatrix} \bar{n}+\alpha\\ \bar{n}-\bar{t} \end{pmatrix} \begin{pmatrix} \bar{n}+\beta\\ \bar{t} \end{pmatrix}, \quad \alpha \geq 0, \quad \beta \geq 0.$$

If m-j or -m-j is negative, then the following symmetry relation can be used to compute $d_{jm}^{(l)}(\pi/2)$:

$$d_{jm}^{(l)}(\varphi) = (-1)^{j-m} d_{mj}^{(l)}(\varphi) = d_{-m-j}^{(l)}(\varphi) = d_{mj}^{(l)}(-\varphi).$$

Combining (5.2)–(5.5) and (4.4), we find that the element $\mathbf{N}_{l'l',li}^{\tilde{k}}$ can be evaluated by

$$\begin{split} \mathbf{N}_{l'j',lj}^{\tilde{k}} &= \sum_{r=0}^{2n+3} \sum_{s=1}^{n+2} \mu_r \nu_s \sum_{r'=0}^{2n'+1} \sum_{s'=1}^{n'+1} \xi_{r'} \eta_{s'} \widetilde{S}_{rsr's'}^{\mathfrak{s}} \\ & \sum_{\tilde{j}=-l}^{l} F_{sl\tilde{j}j} \mathrm{e}^{\mathrm{i}(j-\tilde{j})\varphi_r} \sum_{d=1}^{2} \alpha_{l,j}^{(\tilde{k},d)}(\Theta_{s'}) \mathrm{e}^{\mathrm{i}\tilde{j}\Phi_{r'}} \Big(\mathcal{F}(\hat{y}_{rs}^{r's'}) T_{\hat{x}_{rs}}^{-1} \mathbf{v}^{(d)}(\Theta_{s'}, \Phi_{r'}) \Big) \\ & \cdot \Big(- c_{l'}^{j'} \frac{\partial P_{l'}^{|j'|}(\cos\theta_s)}{\partial \theta_s} \mathrm{e}^{-\mathrm{i}j'\varphi_r} \mathbf{t}_2(\hat{x}_{rs}) - \mathrm{i}j' c_{l'}^{j'} P_{l'}^{|j'|}(\cos\theta_s) \mathrm{e}^{-\mathrm{i}j'\varphi_r} \frac{1}{\sin\theta_s} \mathbf{t}_1(\hat{x}_{rs}) \Big) \end{split}$$

for k' = 1, 2, where

$$\widetilde{S}_{rsr's'}^{\sigma} := \alpha_{s'}^{n'} \widetilde{S}_{1}^{\sigma} (\hat{x}_{rs}, \hat{y}_{rs}^{r's'}) + \widetilde{S}_{2}^{\sigma} (\hat{x}_{rs}, \hat{y}_{rs}^{r's'}), \quad \sigma = \mathfrak{p}, \mathfrak{s},$$

and the element $\mathbf{H}_{l'i',li}^{\tilde{k}}$ is given by

$$\begin{split} \mathbf{H}_{l'j',lj}^{k'} &= \sum_{r=0}^{2n+3} \sum_{s=1}^{n+2} \mu_r \nu_s \sum_{r'=0}^{2n'+1} \sum_{s'=1}^{n'+1} \xi_{r'} \eta_{s'} \widetilde{S}_{rsr's'}^{\mathfrak{p}} \sum_{\tilde{j}=-l}^{l} F_{sl\tilde{j}j} \mathrm{e}^{\mathrm{i}(j-\tilde{j})\varphi_r} c_l^{\tilde{j}} P_l^{|\tilde{j}|} (\cos \Theta_{s'}) \mathrm{e}^{\mathrm{i}j\Phi_{r'}} \\ & \left(\mathbf{t}_1(\hat{\mathbf{x}}_{rs}) \cdot \left[\frac{1}{\sin \theta_s} \frac{\partial \overline{Z}_{l',j'}^{(k')} \circ p(\theta_s, \varphi_r)}{\partial \varphi_r} \right] - \mathbf{t}_2(\hat{\mathbf{x}}_{rs}) \cdot \frac{\partial \overline{Z}_{l',j'}^{(k')} \circ p(\theta_s, \varphi_r)}{\partial \theta_s} \right) \end{split}$$

for $\tilde{k}=1,2$. It can be seen that the direct computation for each element needs $\mathcal{O}(n^4)$ computational cost, which leads to $\mathcal{O}(n^8)$ total computational complexity since there are $\mathcal{O}(n^4)$ matrix elements. To accelerate the evaluation, we adopt the idea of [12,13] and carry out the following operations:

$$\begin{split} E_{srs'\tilde{j}}^{1,d} &= -\sum_{r'=0}^{2n'+1} \xi_{r'} e^{i\tilde{j}\phi_{r'}} \widetilde{S}_{rsr's'}^{\mathfrak{p}} \Big(\mathcal{F}(\hat{y}_{rs}^{r's'}) T_{\hat{x}_{rs}}^{-1} \mathbf{v}^{(d)}(\Theta_{s'}, \Phi_{r'}) \Big) \cdot \mathbf{t}_{2}(\hat{x}_{rs}), \\ E_{srs'\tilde{j}}^{2,d} &= -\sum_{r'=0}^{2n'+1} \xi_{r'} e^{i\tilde{j}\phi_{r'}} \widetilde{S}_{rsr's'}^{\mathfrak{p}} \Big(\mathcal{F}(\hat{y}_{rs}^{r's'}) T_{\hat{x}_{rs}}^{-1} \mathbf{v}^{(d)}(\Theta_{s'}, \Phi_{r'}) \Big) \cdot \mathbf{t}_{1}(\hat{x}_{rs}), \\ D_{srl\tilde{j}}^{\tilde{k},h} &= \sum_{s'=1}^{n'+1} \sum_{d=1}^{2} \eta_{s'} \alpha_{l,\tilde{j}}^{(\tilde{k},d)}(\Theta_{s'}) E_{srs'\tilde{j}}^{h,d}, \quad h = 1, 2, \\ C_{srlj}^{\tilde{k},h} &= \sum_{|\tilde{j}| < l} F_{sl\tilde{j}j} e^{i(j-\tilde{j})\varphi_{r}} D_{srl\tilde{j}}^{\tilde{k},h}, \quad B_{sj'lj}^{\tilde{k},h} &= \sum_{r=0}^{2n+3} \mu_{r} e^{-ij'\varphi_{r}} C_{srlj}^{\tilde{k},h}, \quad h = 1, 2, \end{split}$$

which lead to

$$\mathbf{N}_{l'j',lj}^{\tilde{k}} = \sum_{s=1}^{n+2} \nu_s \Big(c_{l'}^{j'} \frac{\partial P_{l'}^{|j'|}(\cos\theta_s)}{\partial \theta_s} B_{sj'lj}^{\tilde{k},1} + \mathrm{i} j' c_{l'}^{j'} P_{l'}^{|j'|}(\cos\theta_s) \frac{1}{\sin\theta_s} B_{sj'lj}^{\tilde{k},2} \Big).$$

Then the computational complexity reduces to $\mathcal{O}(n^5)$ for $\mathcal{O}(n^4)$ matrix elements, since each operation only requires $\mathcal{O}(n)$ amount of work, which is a great cost saving compared to the original computational complexity $\mathcal{O}(n^8)$.

Similarly, we take the following operations to assemble $\mathbf{H}_{l'i',lj}^{k'}$:

$$\begin{split} E_{srs'\tilde{j}}^{1,d} &= \sum_{r'=0}^{2n'+1} \xi_{r'} e^{i\tilde{j}\Phi_{r'}} \widetilde{S}_{rsr's'}^{\mathfrak{p}} \Big(\mathcal{F}(\hat{x}_{rs}) \boldsymbol{v}^{(d)}(\theta_{s}, \varphi_{r}) \Big) \cdot \boldsymbol{t}_{1}(\hat{x}_{rs}) / \sin\theta_{s}, \\ E_{srs'\tilde{j}}^{2,d} &= \sum_{r'=0}^{2n'+1} \xi_{r'} e^{i\tilde{j}\Phi_{r'}} \widetilde{S}_{rsr's'}^{\mathfrak{p}} \frac{\partial \Big(\mathcal{F}(\hat{x}_{rs}) \boldsymbol{v}^{(d)}(\theta_{s}, \varphi_{r}) \Big)}{\partial \varphi_{r}} \cdot \boldsymbol{t}_{1}(\hat{x}_{rs}) / \sin\theta_{s}, \\ E_{srs'\tilde{j}}^{3,d} &= -\sum_{r'=0}^{2n'+1} \xi_{r'} e^{i\tilde{j}\Phi_{r'}} \widetilde{S}_{rsr's'}^{\mathfrak{p}} \Big(\mathcal{F}(\hat{x}_{rs}) \boldsymbol{v}^{(d)}(\theta_{s}, \varphi_{r}) \Big) \cdot \boldsymbol{t}_{2}(\hat{x}_{rs}), \\ E_{srs'\tilde{j}}^{4,d} &= -\sum_{r'=0}^{2n'+1} \xi_{r'} e^{i\tilde{j}\Phi_{r'}} \widetilde{S}_{rsr's'}^{\mathfrak{p}} \frac{\partial \Big(\mathcal{F}(\hat{x}_{rs}) \boldsymbol{v}^{(d)}(\theta_{s}, \varphi_{r}) \Big)}{\partial \theta_{s}} \cdot \boldsymbol{t}_{2}(\hat{x}_{rs}), \\ D_{srl\tilde{j}}^{w,d} &= \sum_{s'=1}^{n'+1} \eta_{s'} c_{l}^{\tilde{j}} P_{l}^{|\tilde{j}|} (\cos\Theta_{s'}) E_{srs'\tilde{j}}^{w,d}, \quad w = 1, 2, 3, 4, \\ C_{srl\tilde{j}}^{w,d} &= \sum_{|\tilde{j}| \leq l} F_{sl\tilde{j}\tilde{j}} e^{i(j-\tilde{j})\varphi_{r}} D_{srl\tilde{j}}^{w,d}, \quad B_{sj'l\tilde{j}}^{w,d} &= \sum_{r=0}^{2n+3} \mu_{r} e^{-ij'\varphi_{r}} C_{srl\tilde{j}}^{w,d}, \quad w = 1, 2, 3, 4. \end{split}$$

Here we have $\mathcal{F}^{\top}(\hat{x}_{rs}) = [F_1(\hat{x}_{rs}), F_2(\hat{x}_{rs}), F_3(\hat{x}_{rs})]$, and then

$$\frac{\partial}{\partial \theta_{s}} \Big(\mathcal{F}(\hat{\mathbf{x}}_{rs}) \mathbf{v}^{(d)}(\theta_{s}, \varphi_{r}) \Big) = \begin{bmatrix} \partial_{\theta_{s}} F_{1}(\hat{\mathbf{x}}_{rs}) \cdot \mathbf{v}^{(d)}(\theta_{s}, \varphi_{r}) + F_{1}(\hat{\mathbf{x}}_{rs}) \cdot \partial_{\theta_{s}} \mathbf{v}^{(d)}(\theta_{s}, \varphi_{r}) \\ \partial_{\theta_{s}} F_{2}(\hat{\mathbf{x}}_{rs}) \cdot \mathbf{v}^{(d)}(\theta_{s}, \varphi_{r}) + F_{2}(\hat{\mathbf{x}}_{rs}) \cdot \partial_{\theta_{s}} \mathbf{v}^{(d)}(\theta_{s}, \varphi_{r}) \\ \partial_{\theta_{s}} F_{3}(\hat{\mathbf{x}}_{rs}) \cdot \mathbf{v}^{(d)}(\theta_{s}, \varphi_{r}) + F_{3}(\hat{\mathbf{x}}_{rs}) \cdot \partial_{\theta_{s}} \mathbf{v}^{(d)}(\theta_{s}, \varphi_{r}) \end{bmatrix}.$$

One can analogously obtain $\frac{\partial}{\partial \varphi_r} \Big(\mathcal{F}(\hat{x}_{rs}) \boldsymbol{v}^{(d)}(\theta_s, \varphi_r) \Big)$. Then $\mathbf{H}_{l'j',lj}^{k'}$ can be evaluated by

$$\mathbf{H}_{l'j',lj}^{k'} = \sum_{s=1}^{n+2} \sum_{d=1}^{2} \nu_{s} \left(\overline{ij'\alpha_{l',j'}^{(k',d)}(\theta_{s})} B_{sj'lj}^{1,d} + \overline{\alpha_{l',j'}^{(k',d)}(\theta_{s})} B_{sj'lj}^{2,d} + \overline{\frac{\partial \alpha_{l',j'}^{(k',d)}(\theta_{s})}{\partial \theta_{s}}} B_{sj'lj}^{3,d} + \overline{\alpha_{l',j'}^{(k',d)}(\theta_{s})} B_{sj'lj}^{4,d} \right).$$

It is worth pointing out that the numerical implementation can be done very efficiently since each step of the operations only involves scalar functions.

We briefly mention the evaluation of $\mathbf{U}_{l'j',lj}^{k',\tilde{k}}$ and $\mathbf{I}_{l'j',lj}$. Noting that \mathcal{F} is an orthogonal transformation, we may obtain $\mathbf{U}_{l'j',lj}^{k',\tilde{k}}$ via

$$C_{srlj}^{\tilde{k},d'} = \alpha_{l,j}^{(\tilde{k},d')}(\theta_{s})e^{ij\varphi_{r}}J_{\mathbf{q}} \circ p(\theta_{s},\varphi_{r}), \quad B_{sj'lj}^{\tilde{k},d'} = \sum_{r=0}^{2n+3} \mu_{r}e^{-ij'\varphi_{r}}C_{srlj}^{\tilde{k},d'}, \quad \tilde{k},d' = 1,2,$$

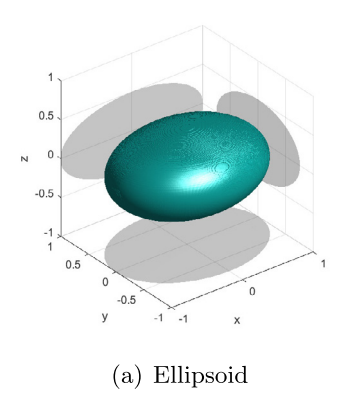
$$\mathbf{U}_{l'j',lj}^{k',\tilde{k}} = \sum_{s=1}^{n+2} \sum_{d'=1}^{2} \nu_{s}\overline{\alpha_{l',j'}^{(k',d')}(\theta_{s})}B_{sj'lj}^{\tilde{k},d'},$$

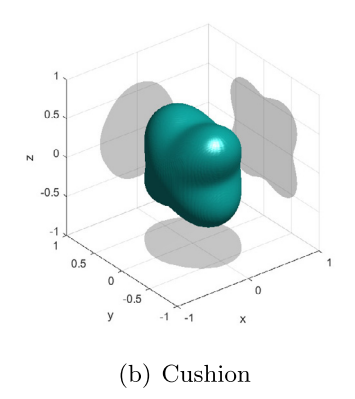
and $\mathbf{I}_{l'j',lj}$ via

$$C_{srlj} = c_l^j P_l^{|j|}(\cos \theta_s) e^{ij\varphi_r} J_{\mathbf{q}} \circ p(\theta_s, \varphi_r), \quad B_{sj'lj} = \sum_{r=0}^{2n+3} \mu_r e^{-ij'\varphi_r} C_{srlj},$$

$$\mathbf{I}_{l'j',lj} = \sum_{r=1}^{n+2} \nu_s c_{l'}^{j'} P_{l'}^{|j'|}(\cos \theta_s) B_{sj'lj}.$$

The approximations $\mathbf{K}_{l'j',lj}$ and $\mathbf{M}_{l'j',lj}^{k',\hat{k}}$ for \mathcal{K} and \mathcal{M} are discussed in [12,13], and we give them in the appendix with slight modifications.





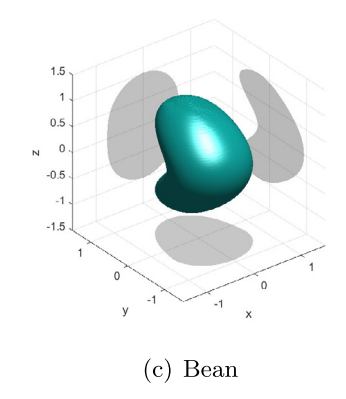


Fig. 1. Geometries of the obstacles.

Table 1 Parametrizations of the obstacles.

Type	Parametrization
Ellipsoid Cushion	$x_1^2 + \frac{x_2^2}{0.75^2} + \frac{x_3^2}{0.5^2} = 1$ $x(\theta, \varphi) = \sqrt{0.27 + 0.065(\cos 2\varphi - 1)(\cos 4\theta - 1)}\hat{x}(\theta, \varphi)$
Bean	$\frac{x_1^2}{0.64(1 - 0.1\cos(\pi x_3))} + \frac{(0.3\cos(\pi x_3) + x_2)^2}{0.64(1 - 0.4\cos(\pi x_3))} + x_3^2 = 1$

Table 2 Numerical results for the ellipsoid-shaped obstacle at $\omega = \pi$.

	Ellipsoid: $\omega =$	π		
n	$ \epsilon_{ps} _{\infty}$	$ \epsilon_{pw} _{\infty}$	T_{coe}	T_{sol}
5	2.0854e-04	7.8646e-03	0.2 s	0.0003 s
15	2.1597e-08	6.7751e-08	2.9 s	0.008 s
25	2.6595e-12	3.6123e-11	16.8 s	0.1 s
35	2.9117e-14	3.3012e-11	64.3 s	0.5 s
45	5.8231e-14	3.0243e-11	239.8 s	2.0 s
55	4.4362e-14	4.0796e-11	874.4 s	6.1 s

Remark 5.1. The convergence analysis of the proposed numerical method depends on the invertibility of the boundary integral system (3.5) as well as the discretized system (5.1), which is beyond the scope of this paper and currently under investigation. We refer to [7] for the convergence analysis for the two-dimensional problems. It is expected that the following estimate holds under certain conditions:

$$||(\widetilde{G}^n_{\mathfrak{p}} \circ \boldsymbol{q}^{-1}, \widetilde{G}^n_{\mathfrak{s}} \circ \boldsymbol{q}^{-1})^\top - (g_1, \boldsymbol{g}_2)^\top||_{\infty, \Gamma_D} \leq \frac{C}{n^q} ||(g_1, \boldsymbol{g}_2)^\top||_{q+1, \infty, \Gamma_D}, \quad \forall q \in \mathbb{N},$$

where $(g_1, \mathbf{g}_2)^{\top}$ is the exact solution to the integral equation system (3.6), $||\cdot||_{\infty,\Gamma_D}$ is the maximum norm for functions in $C(\Gamma_D) \times \mathbf{C}_T(\Gamma_D)$, and $||\cdot||_{q,\infty,\Gamma_D}$ is the norm for continuously differentiable vector functions on Γ_D up to order q. Numerical experiments show that the spectral convergence is achieved as long as $n' \geq 2n + 1$ with sufficiently large n.

6. Numerical experiments

In this section, we present some numerical experiments to demonstrate the superior performance of the proposed method. We consider three different geometries for the obstacle: ellipsoid, cushion, and bean, as shown in Fig. 1. Their parametrizations are given in Table 1. Throughout the numerical experiments, we take the Lamé parameters $\lambda=2$, $\mu=1$ and the truncation number n'=2n+1. The method is implemented using MATLAB on a server with two Intel Xeon cores and 256 GB RAM. No special effort is paid to solving the resulted linear system of equations other than the *backslash* command in MATLAB.

To test the accuracy of the proposed method, we construct an exact solution in form of

$$\mathbf{v}_{*}(x) = \mathbb{G}(x, y_0)\mathbf{p}, \quad y_0 = (0, 0.05, 0.0866)^{\top}, \quad \mathbf{p} = (1, 0, 0)^{\top},$$
 (6.1)

Table 3 Numerical results for the cushion-shaped obstacle at $\omega = \pi$.

	Cushion: $\omega = \pi$			
n	$ \epsilon_{ps} _{\infty}$	$ \epsilon_{pw} _{\infty}$	T_{coe}	T_{sol}
5	3.2246e-04	3.9169e-02	0.3 s	0.0003 s
15	8.9083e-07	5.4441e-06	3.3 s	0.009 s
25	1.5665e-09	4.1725e-08	17.5 s	0.1 s
35	1.0287e-11	3.6207e-10	67.1 s	0.5 s
45	2.4172e-13	3.6305e-11	254.1 s	2.1 s
55	6.2876e-14	4.5173e-11	930.5 s	7.0 s

Table 4Numerical results for the bean-shaped obstacle at $\omega = \pi$.

	Bean: $\omega = \pi$			
n	$ \epsilon_{ps} _{\infty}$	$ \epsilon_{pw} _{\infty}$	T_{coe}	T_{sol}
5	4.7523e-03	1.4119e-01	0.2 s	0.0003 s
15	4.8644e-05	1.7490e-04	3.2 s	0.008 s
25	2.4575e-07	1.7558e-06	18.0 s	0.1 s
35	3.3519e-09	2.1805e-08	66.3 s	0.5 s
45	8.9240e-11	9.1735e-11	237.5 s	2.2 s
55	2.9727e-11	7.0980e-11	905.0 s	5.9 s

Table 5 Scattering by an ellipsoid-shaped obstacle at $\omega = 8\pi$.

	Ellipsoid: $\omega = 8\pi$		
n	$ \epsilon_{ps} _{\infty}$	$\Re\{\boldsymbol{v}_{n,pw}^{\infty}(\boldsymbol{d})\cdot\boldsymbol{p}\}$	$\Im\{\boldsymbol{v}_{n,pw}^{\infty}(\boldsymbol{d})\cdot\boldsymbol{p}\}$
25	3.6217e-05	-1.564489047510042e+00	1.051655398026258e+01
30	1.1212e-07	-1.564570656025764e+00	1.051657743451597e+01
35	2.7707e-10	-1.564570705114201e+00	1.051657744366693e+01
40	1.9588e-12	-1.564570705195090e+00	1.051657744366860e+01
45	5.0535e-13	-1.564570705193652e+00	1.051657744366452e+01

which is the same as the first test in [19], where the tensor

$$\mathbb{G}(x, y) = \frac{1}{\mu} \Big(\Phi(x, y; \kappa_{\mathfrak{s}}) I + \frac{1}{\kappa_{\mathfrak{s}}^2} \nabla_x \nabla_x^\top \Big(\Phi(x, y; \kappa_{\mathfrak{s}}) - \Phi(x, y; \kappa_{\mathfrak{p}}) \Big) \Big)$$

is the fundamental solution of the elastic wave equation and $\Phi(x, y, \kappa)$ is the fundamental solution for the three-dimensional Helmholtz equation given in (3.1). Then, the corresponding far-field is given by

$$\boldsymbol{v}_{\boldsymbol{*},\boldsymbol{ps}}^{\infty}(\hat{\boldsymbol{x}}) = \frac{1}{\mu} \frac{\mathrm{e}^{-\mathrm{i}\kappa_{\mathfrak{s}}\hat{\boldsymbol{x}}\cdot\boldsymbol{y}_{0}}}{4\pi} (\hat{\boldsymbol{x}}\times\boldsymbol{p}) \times \hat{\boldsymbol{x}} + \frac{1}{\lambda + 2\mu} \frac{\mathrm{e}^{-\mathrm{i}\kappa_{\mathfrak{p}}\hat{\boldsymbol{x}}\cdot\boldsymbol{y}_{0}}}{4\pi} (\hat{\boldsymbol{x}}\cdot\boldsymbol{p})\hat{\boldsymbol{x}}.$$

Due to the uniqueness result given in Theorem 2.1, we can solve the boundary value problem (2.4) by enforcing the following boundary conditions on Γ_D :

$$u = v_{*}$$

Then, the numerical far-field pattern $\mathbf{v}_n^{\infty} = \mathbf{v}_{n,\mathfrak{p}}^{\infty} + \mathbf{v}_{n,\mathfrak{s}}^{\infty}$ can be calculated by using (2.8) and (3.4). The maximum errors are calculated over 1300 observations (equally spaced for the observation angles θ and φ) in accordance with the expression

$$\|\epsilon_{ps}\|_{\infty} := \|\boldsymbol{v}_{n,ps}^{\infty} - \boldsymbol{v}_{*,ps}^{\infty}\|_{\infty} = \max_{\hat{v} \in \mathbb{Q}^2} |\boldsymbol{v}_{n,ps}^{\infty}(\hat{x}) - \boldsymbol{v}_{*,ps}^{\infty}(\hat{x})|.$$

In addition to the point source case, we also compute the far-field pattern, denoted by \mathbf{v}_{pw}^{∞} , resulted from the elastic plane wave incidence

$$\boldsymbol{u}^{i}(x) = \frac{1}{\mu} e^{i\kappa_{\mathfrak{g}} x \cdot \boldsymbol{d}} (\boldsymbol{d} \times \boldsymbol{p}) \times \boldsymbol{d} + \frac{1}{\lambda + 2\mu} e^{i\kappa_{\mathfrak{p}} x \cdot \boldsymbol{d}} (\boldsymbol{d} \cdot \boldsymbol{p}) \boldsymbol{d}, \quad \boldsymbol{d}, \, \boldsymbol{p} \in \mathbb{S}^{2},$$

$$(6.2)$$

where the incident direction vector $\mathbf{d} = (0, 0, 1)^{\top}$ and the polarization vector $\mathbf{p} = (1, 0, 0)^{\top}$. Again, we calculate the maximum errors over the observations on the unit sphere by using

$$\|\epsilon_{pw}\|_{\infty} := \|\boldsymbol{v}_{n,pw}^{\infty} - \boldsymbol{v}_{n_*,pw}^{\infty}\|_{\infty} = \max_{\hat{\boldsymbol{x}} \in \mathbb{S}^2} |\boldsymbol{v}_{n,pw}^{\infty}(\hat{\boldsymbol{x}}) - \boldsymbol{v}_{n_*,pw}^{\infty}(\hat{\boldsymbol{x}})|,$$

where n_* is a sufficiently large number.

Table 6 Scattering by a cushion-shaped obstacle at $\omega = 8\pi$.

	Cushion: $\omega = 8\pi$		
n	$ \epsilon_{ps} _{\infty}$	$\Re\{\boldsymbol{v}_{n,pw}^{\infty}(\boldsymbol{d})\cdot\boldsymbol{p}\}$	$\Im\{\boldsymbol{v}_{n,pw}^{\infty}(\boldsymbol{d})\cdot\boldsymbol{p}\}$
25	2.5022e-04	-1.569712590870811e+00	5.039800881189093e+00
30	1.0344e-05	-1.574459019608859e+00	5.043376519089912e+00
35	2.6371e-07	-1.574531401615982e+00	5.043437889542368e+00
40	1.4952e-08	-1.574531761370081e+00	5.043437868795261e+00
45	1.5917e-09	-1.574531768527667e+00	5.043437902490211e+00
50	1.7031e-10	-1.574531769006316e+00	5.043437900206628e+00

Table 7 Scattering by a bean-shaped obstacle at $\omega = 8\pi$.

	Bean: $\omega = 8\pi$		
n	$ \epsilon_{ps} _{\infty}$	$\Re\{\boldsymbol{v}_{n,pw}^{\infty}(\boldsymbol{d})\cdot\boldsymbol{p}\}$	$\Im\{\boldsymbol{v}_{n,pw}^{\infty}(\boldsymbol{d})\cdot\boldsymbol{p}\}$
35	1.7121e-02	-2.387421716629113e+00	1.012728600300475e+01
40	1.5762e-03	-2.385302268097332e+00	1.011101559995000e+01
45	1.2892e-04	-2.384320155063459e+00	1.010913376752758e+01
50	3.4649e-06	-2.384311423020166e+00	1.010898949549377e+01
55	1.9260e-07	-2.384312575610280e+00	1.010899080953868e+01

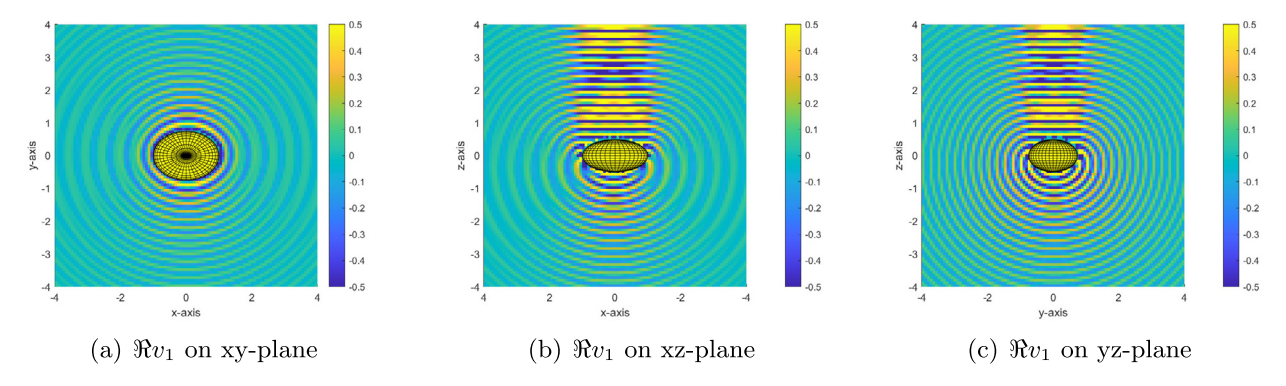


Fig. 2. The scattered field \mathbf{v} for the ellipsoid-shaped obstacle with $\omega = 8\pi$.

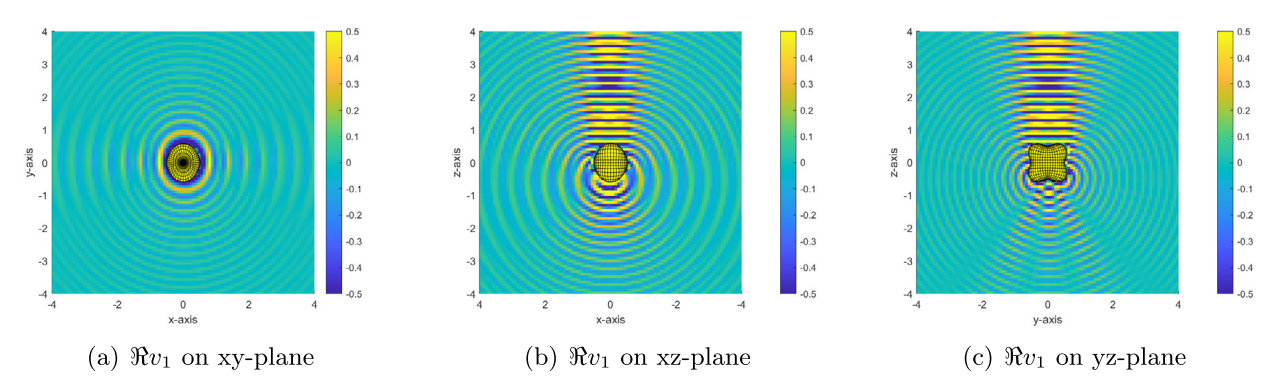


Fig. 3. The scattered field \mathbf{v} for the cushion-shaped obstacle with $\omega = 8\pi$.

6.1. Example 1

In this example, we evaluate the elastic scattering problem for three different obstacles at the frequency $\omega=\pi$. We choose $n_*=60$ when the analytical solution is not available. Numerical results for the ellipsoid-shaped obstacle are given in Table 2. It is shown that the solver rapidly achieves 13 digits accuracy for the point source test with n=35 and stops increasing due to the round off errors. For the plane wave scattering, 10 digits accuracy is obtained with n=25. Table 2 also shows the time to construct the scattering matrix, denoted by T_{coe} in seconds, and the time to solve the linear system, denoted by T_{sol} in seconds. It is clear to note that the time is dominated by the matrix construction and roughly scales on the order of $\mathcal{O}(n^5)$, which is consistent with our complexity analysis. Tables 3 and 4 give the numerical results for the

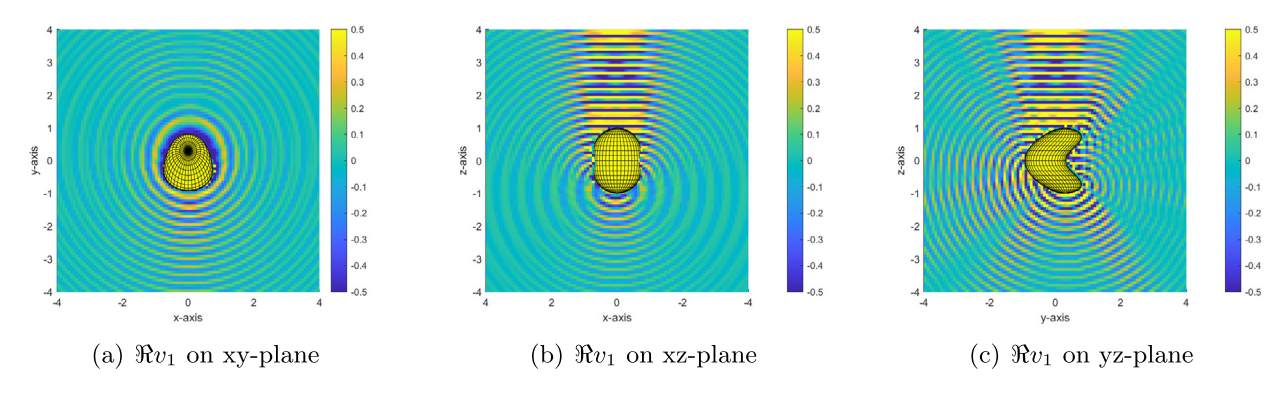


Fig. 4. The scattered field ${\bf v}$ for the bean-shaped obstacle with $\omega=8\pi$.

 Table 8

 Elastic scattering for the ellipsoid-shaped obstacle at high frequencies.

	Ellipsoid: $ \epsilon_{ps} _{\infty}$			
ω	n = 75	n = 80	n = 85	
16π	1.2813e-11	2.8726e-12	4.4200e-11	
24π	3.0964e-05	1.3045e-07	2.2170e-10	

Table 9 Elastic scattering for the cushion-shaped obstacle at high frequencies.

Cushion: $ \epsilon_{ps} _{\infty}$			
ω	n = 75	n = 80	n = 85
16π	9.5257e-10	4.5437e-10	4.0872e-09
24π	1.5524e-05	8.9533e-07	3.0466e-08

cushion- and bean-shaped obstacles, respectively. Both tables show a rapid convergence as n increases, which confirms the spectral accuracy of the solver.

6.2. Example 2

We consider the elastic scattering of three obstacles at higher frequency $\omega=8\pi$. The real and the imaginary parts of the quantity $\mathbf{v}_{n,pw}^{\infty}(\mathbf{d}) \cdot \mathbf{p}$, together with the errors $\|\epsilon_{ps}\|_{\infty}$ for three obstacles are shown in Tables 5, 6, and 7, respectively. Similarly, we observe a rapid convergence both for the point source test and plane wave scattering when n increases. For a fixed n, the accuracy for the scattering of the ellipsoid is higher than that of the cushion and bean. This is due to the reason that the convergence rate depends on the smoothness of the obstacle boundary [15] and it is expected that a less smooth boundary will lead to slower convergence rate. In Fig. 2, Fig. 3 and Fig. 4, we show the real part of the first component of the scattered field $\mathbf{v}=(v_1,v_2,v_3)^{\top}$, i.e. $\Re v_1$, generated by a plane wave $\mathbf{u}^i(x)$ with $\mathbf{d}=(0,0,1)^{\top}$ and $\mathbf{p}=(1,0,0)^{\top}$ in (6.2) for ellipsoid-, cushion- and bean-shaped obstacles, respectively.

6.3. Example 3

In this example, we consider the high frequency scattering problem, which is challenging due to the high oscillation of the solution. In particular, we apply the spectral method to test the point source scattering by the ellipsoid and cushion at $\omega=16\pi$ and $\omega=24\pi$, respectively. Numerical errors for the two obstacles with different discretization number n are shown in Tables 8 and 9. It can be seen that the high order convergence can still be achieved at high frequencies, which demonstrates that the solver is robust for the scattering problem in both low and high frequencies.

7. Conclusion

In this paper, we have proposed a novel boundary integral formulation and developed a high order spectral method for solving the elastic obstacle scattering problem in three dimensions. Based on the Helmholtz decomposition, the elastic scattering problem is reduced to a coupled boundary value problem. The uniqueness is examined for both the coupled boundary value problem and the system of boundary integral equations. By making use of the surface differential operators and Stokes' formula, we reduce the strongly singular operators to a weakly singular operator in form of the exterior integral of the Galerkin method. In addition, all operations in the full discretization are scalar, which makes the numerical

implementation much simpler. Numerical experiments, including three different obstacles and high frequency scattering, are shown to demonstrate the superior performance of the proposed method. Future work includes the convergence analysis of the proposed method, the extension to other boundary conditions, and applications to solve the inverse elastic scattering problems.

Declaration of competing interest

The authors declare that they have no known competing financial interests or personal relationships that could have appeared to influence the work reported in this paper.

Appendix A

Here we give the approximations $\mathbf{K}_{l'j',lj}$ and $\mathbf{M}_{l'j',lj}^{k',\tilde{k}}$ for \mathcal{K} and \mathcal{M} with a slight modification. Details can be found in [12,13]. The approximation $\mathcal{K}_{n'}$ to \mathcal{K} can be simplified as

$$\begin{split} (\mathcal{K}_{n'}G)(\hat{x}) &:= \int\limits_{\mathbb{S}^2} \Big(\frac{1}{|\hat{n} - \hat{z}|} \mathcal{L}_{n'}^{\mathfrak{p}} \big\{ T_{\hat{x}} \widetilde{K}_{1}(\hat{n}, \hat{z}) T_{\hat{x}} G(\hat{z}) \big\} + \mathcal{L}_{n'}^{\mathfrak{p}} \big\{ T_{\hat{x}} \widetilde{K}_{2}(\hat{n}, \hat{z}) T_{\hat{x}} G(\hat{z}) \big\} \Big) \, \mathrm{d}s(\hat{z}) \\ &= \sum_{l=0}^{n'} \sum_{|j| \leq l} \frac{4\pi}{2l+1} \Big(T_{\hat{x}} \widetilde{K}_{1}(\hat{n}, \cdot) T_{\hat{x}} G(\cdot), Y_{l,j}(\cdot) \Big)_{n'} Y_{l,j}(\hat{n}) \\ &+ \sum_{l=0}^{n'} \sum_{|j| \leq l} \Big(T_{\hat{x}} \widetilde{K}_{2}(\hat{n}, \cdot) T_{\hat{x}} G(\cdot), Y_{l,j}(\cdot) \Big)_{n'} Y_{l,j}(\hat{n}) \\ &= \sum_{r'=0}^{2n'+1} \sum_{s'=1}^{n'} \xi_{r'} \eta_{s'} \Big[\alpha_{s'}^{n'} T_{\hat{x}} \widetilde{K}_{1,d}(\hat{n}, \hat{y}_{r's'}) + T_{\hat{x}} \widetilde{K}_{2,d}(\hat{n}, \hat{y}_{r's'}) \Big] T_{\hat{x}} G(\hat{y}_{r's'}). \end{split}$$

Then we obtain

$$\begin{split} \mathbf{K}_{l'j',lj} = & (\mathcal{K}_{n'}Y_{l,j}, Y_{l',j'})_{n+1} \\ = & \sum_{r=0}^{2n+3} \sum_{s=1}^{n+2} \mu_r \nu_s \sum_{r'=0}^{2n'+1} \sum_{s'=1}^{n'+1} \xi_{r'} \eta_{s'} \Big[\alpha_{s'}^{n'} \widetilde{K}_1(\hat{\mathbf{x}}_{rs}, \hat{\mathbf{y}}_{rs}^{r's'}) + \widetilde{K}_2(\hat{\mathbf{x}}_{rs}, \hat{\mathbf{y}}_{rs}^{r's'}) \Big] \\ & \times \sum_{|\tilde{j}| \leq l} F_{sl\tilde{j}j} \mathrm{e}^{\mathrm{i}(j-\tilde{j})\varphi_r} Y_{l,\tilde{j}} \Big(p(\Theta_{s'}, \Phi_{r'}) \Big) \overline{Y_{l',j'} \Big(p(\theta_s, \varphi_r) \Big)} \end{split}$$

via the operations

$$\begin{split} E_{srs'\tilde{j}}^{1} &= \sum_{r'=0}^{2n'+1} \xi_{r'} \widetilde{K}_{1}(\hat{x}_{rs}, \hat{y}_{rs}^{r's'}) e^{i\tilde{j}\Phi_{r'}}, \quad E_{srs'\tilde{j}}^{2} = \sum_{r'=0}^{2n'+1} \xi_{r'} \widetilde{K}_{2}(\hat{x}_{rs}, \hat{y}_{rs}^{r's'}) e^{i\tilde{j}\Phi_{r'}}, \\ D_{srl\tilde{j}} &= \sum_{s'=1}^{n'+1} \eta_{s'} \left[\alpha_{s'}^{n'} E_{srs'\tilde{j}}^{1} + E_{srs'\tilde{j}}^{2} \right] c_{l}^{\tilde{j}} P_{l}^{|\tilde{j}|}(\cos \Theta_{s'}), \\ C_{srlj} &= \sum_{|\tilde{j}| \leq l} D_{srl\tilde{j}} F_{sl\tilde{j}j} e^{i(j-\tilde{j})\varphi_{r}}, \quad B_{sj'lj} = \sum_{r=0}^{2n+3} C_{srlj} \mu_{r} e^{-ij'\varphi_{r}}, \\ \mathbf{K}_{l'j',lj} &= \sum_{s=1}^{n+2} B_{sj'lj} \nu_{s} c_{l'}^{j'} P_{l'}^{|j'|}(\cos \theta_{s}). \end{split}$$

Analogously, the entry of $\mathbf{M}_{l'j',lj}^{k',\tilde{k}}$ can be obtained via the following operations:

$$E_{srs'\tilde{j}}^{d,d'} = \sum_{r'=0}^{2n'+1} \xi_{r'} e^{i\tilde{j}\boldsymbol{\Phi}_{r'}} \boldsymbol{v}^{(d')}(\theta_s, \varphi_r)^{\top} \mathcal{F}^{\top}(\hat{x}_{rs}) M_{n'}(\hat{x}_{rs}, \hat{y}_{rs}^{r's'}) \mathcal{F}(\hat{x}_{rs}) T_{\hat{x}_{rs}}^{-1} \boldsymbol{v}^{(d)}(\Theta_{s'}, \boldsymbol{\Phi}_{r'}),$$

$$\begin{split} &D_{srl\tilde{j}}^{\tilde{k},d'} = \sum_{s'=1}^{n'+1} \sum_{d=1}^{2} \eta_{s'} \alpha_{l,\tilde{j}}^{(\tilde{k},d)}(\Theta_{s'}) E_{srs'\tilde{j}}^{d,d'}, \\ &C_{srlj}^{\tilde{k},d'} = \sum_{|\tilde{j}| \leq l} F_{sl\tilde{j}j} \mathrm{e}^{\mathrm{i}(j-\tilde{j})\varphi_r} D_{srl\tilde{j}}^{\tilde{k},d'}, \quad B_{sj'lj}^{\tilde{k},d'} = \sum_{r=0}^{2n+3} \mu_r \mathrm{e}^{-\mathrm{i}j'\varphi_r} C_{srlj}^{\tilde{k},d'}, \\ &\mathbf{M}_{l'j',lj}^{k',\tilde{k}} = \sum_{s=1}^{n+2} \sum_{d'=1}^{2} \nu_s \overline{\alpha_{l',j'}^{(k',d')}(\theta_s)} B_{sj'lj}^{\tilde{k},d'}, \end{split}$$

where $M_{n'}(\hat{x}_{rs}, \hat{y}_{rs}^{r's'}) = \alpha_{s'}^{n'} \widetilde{M}_1(\hat{x}_{rs}, \hat{y}_{rs}^{r's'}) + \widetilde{M}_2(\hat{x}_{rs}, \hat{y}_{rs}^{r's'})$, and $\widetilde{M}_1(\hat{x}, \hat{y})$, $\widetilde{M}_2(\hat{x}, \hat{y})$ are 3×3 matrices defined in (4.5). In contrast to the operations in [12], which put $\mathbf{v}^{(d')^{\top}}$ in $\mathbf{B}_{sj't'lj\tilde{k}}$, we combine $\mathbf{v}^{(d')^{\top}}$ and \mathcal{F}^{\top} together so that $E_{srs'\tilde{j}}^{d,d'}$ is a scalar function, which makes the numerical implementation simpler since each operation is scalar.

References

- [1] H. Ammari, E. Bretin, J. Garnier, H. Kang, H. Lee, A. Wahab, Mathematical Methods in Elasticity Imaging, Princeton University Press, New Jersey, 2015.
- [2] G. Bao, L. Xu, T. Yin, An accurate boundary element method for the exterior elastic scattering problem in two dimensions, J. Comput. Phys. 348 (2017) 343–363.
- [3] O.P. Bruno, T. Yin, Regularized integral equation methods for elastic scattering problems in three dimensions, J. Comput. Phys. 410 (2020) 109350.
- [4] F. Bu, J. Lin, F. Reitich, A fast and high-order method for the three-dimensional elastic wave scattering problems, J. Comput. Phys. 258 (2014) 856–870.
- [5] D. Colton, R. Kress, Integral Equation Methods in Scattering Theory, SIAM, Philadelphia, 2013.
- [6] D. Colton, R. Kress, Inverse Acoustic and Electromagnetic Scattering Theory, third edition, Springer, New York, 2013.
- [7] H. Dong, J. Lai, P. Li, A highly accurate boundary integral method for the elastic obstacle scattering problem, Math. Comput. 90 (2021) 2785–2814.
- [8] H. Dong, J. Lai, P. Li, An inverse acoustic-elastic interaction problem with phased or phaseless far-field data, Inverse Probl. 36 (2020) 035014.
- [9] H. Dong, J. Lai, P. Li, Inverse obstacle scattering for elastic waves with phased or phaseless far-field data, SIAM J. Imaging Sci. 12 (2019) 809-838.
- [10] M. Ganesh, I.G. Graham, A high-order algorithm for obstacle scattering in three dimensions, J. Comput. Phys. 198 (2004) 211-242.
- [11] M. Ganesh, S.C. Hawkins, A hybrid high-order algorithm for radar cross section computations, SIAM J. Sci. Comput. 29 (2007) 1217-1243.
- [12] M. Ganesh, S.C. Hawkins, A high-order tangential basis algorithm for electromagnetic scattering by curved surface, J. Comput. Phys. 227 (2008) 4543–4562.
- [13] I.G. Graham, I.H. Sloan, Fully discrete spectral boundary integral methods for Helmholtz problems on smooth closed surfaces in \mathbb{R}^3 , Numer. Math. 92 (2002) 289–323.
- [14] L. Greengard, S. Jiang, A new mixed potential representation for the equations of unsteady, incompressible flow, SIAM Rev. 61 (2019) 733-755.
- [15] R. Kress, Linear Integral Equations, third edition, Springer, 2010.
- [16] L.D. Landau, E.M. Lifshitz, Theory of Elasticity, Pergamon, Oxford, 1986.
- [17] P. Li, X. Yuan, Inverse obstacle scattering for elastic waves in three dimensions, Inverse Probl. Imaging 13 (2019) 545-573.
- [18] Y. Liu, F.J. Rizzo, Hypersingular boundary integral equations for radiation and scattering of elastic waves in three dimensions, Comput. Methods Appl. Mech. Eng. 107 (1993) 131–144.
- [19] F.L. Louër, A high order spectral algorithm for elastic obstacle scattering in three dimensions, J. Comput. Phys. 279 (2014) 1-17.
- [20] F.L. Louër, A spectrally accurate method for the dielectric obstacle scattering problem and applications to the inverse problem, arXiv:2006.10830, 2020.
- [21] S.G. Mikhlin, S. Prössdorf, Singular Integral Operators, Springer Verlag, Berlin, 1986.
- [22] J.C. Nédélec, Acoustic and Electromagnetic Equations: Integral Representations for Harmonic Problems, Springer, New York, 2000.
- [23] Y.H. Pao, V. Varatharajulu, Huygens' principle, radiation conditions, and integral formulas for the scattering of elastic waves, J. Acoust. Soc. Am. 59 (1976) 1361–1371
- [24] M.S. Tong, W.C. Chew, Nyström method for elastic wave scattering by three-dimensional obstacles, J. Comput. Phys. 226 (2007) 1845-1858.
- [25] J. Yue, M. Li, P. Li, X. Yuan, Numerical solution of an inverse obstacle scattering problem for elastic waves via the Helmholtz decomposition, Commun. Comput. Phys. 26 (2019) 809–837.